Computer Methods in Applied Mechanics and Engineering 199 (2010) 1881–1905

Contents lists available at ScienceDirect

Computer Methods in Applied Mechanics and Engineering

journal homepage: www.elsevier.com/locate/cma

A multi-level wave based numerical modelling framework for the steady-state dynamic analysis of bounded Helmholtz problems with multiple inclusions

Bert Van Genechten *, Karel Vergote, Dirk Vandepitte, Wim Desmet

K.U. Leuven - Dept. of Mechanical Engineering, Celestijnenlaan 300B - box 2420, 3001 Heverlee (Leuven), Belgium

ARTICLE INFO

Article history:
Received 7 October 2009
Received in revised form 6 January 2010
Accepted 25 January 2010
Available online 6 March 2010

Keywords:
Multiple inclusions
Helmholtz equation
Acoustics
Elastodynamics
Mid-frequency
Wave Based Method

ABSTRACT

The Wave Based Method (WBM) is an alternative numerical prediction method for both interior and exterior steady-state dynamic problems, which is based on an indirect Trefftz approach. It applies wave functions, which are exact solutions of the governing differential equation, to describe the dynamic field variables. The smaller system of equations and the absence of pollution errors make the WBM very suitable for the treatment of Helmholtz problems in the mid-frequency range, where element-based methods are no longer feasible due to the associated computational costs. A sufficient condition for convergence of the method is the convexity of the considered problem domain. As a result, only problems of moderate geometrical complexity can be considered and some geometrical features cannot be handled at all. In this paper, these limitations are alleviated through the development of a general modelling framework based on existing WBM methodologies which allows for the efficient introduction of inclusion configurations in bounded WBM models for problems governed by one or more Helmholtz equations. The feasibility and efficiency of the method is illustrated by means of numerical verification studies in which the methodology is applied to two types of dynamic problems. On the one hand, a single Helmholtz equation associated with the steady-state dynamic behaviour of acoustic cavities is studied. On the other hand, the framework is applied to the solution of the Navier system of partial differential equations that describe the elastodynamic response of two-dimensional perforated solids.

1. Introduction

In recent years, the application of numerical simulation techniques in design, analysis and optimisation of mechanical systems has become an indispensable part of the industrial design process. Both the Finite Element Method (FEM) and the Boundary ElementMethod (BEM) are well established Computer Aided Engineering (CAE) tools which are commonly used for the analysis of time-harmonic dynamic problems.

The FEM [1] discretises the problem domain into a large but finite number of small elements. Within these elements, the dynamic field variables are described in terms of simple, polynomial shape functions. However, since these shape functions are no exact solutions of the governing differential equations, a fine discretisation is required to suppress the associated pollution error [2] and to obtain reasonable prediction accuracy at higher frequencies. Solving the resulting large numerical models requires a prohibitively large amount of computational resources. As a result, the FEM is limited to low-frequency applications [3].

In recent years, a vast amount of research has been done into the development of possible extensions of the FEM in order to minimise or even eliminate the numerical pollution effects and, as a result, increase the practical application range of the method to higher frequencies. This has lead to a wide range of techniques, which can be classified into a number of categories based on their specific focus. A first family of approaches attempts to optimise the FE modelling process without fundamentally altering it. Among these, refinement methods aim at reducing the approximation errors through adaptive (local) reduction of the dimensions of the FE discretisation [2] or through an elevation of the approximation order of the FEM basis functions [4] or through a combination of both [5]. Alternatively, [6–9] propose special numerical integration schemes which significantly increase the accuracy of the FEM with respect to numerical pollution errors. Advanced iterative solution strategies can also be employed to solve the FE numerical models more efficiently [10,11]. The main drawback of these solution algorithms is that they are less robust and that the gain in computational efficiency is highly dependent on the problem at hand and the combination of iterative solver and preconditioner used to solve the numerical systems. Domain decomposition techniques, like Component Mode Synthesis [12], its automated iterative variation Automated Multi-Level Substructuring [13,14] and the Finite Element Tearing and Interconnecting approach [15,16], apply a *divide and conquer* strategy which is perfectly suited

* Corresponding author. Tel.: +32 16 32 86 06; fax: +32 16 32 29 87.
E-mail address: Bert.VanGenechten@mech.kuleuven.be (B. Van Genechten).

0045-7825/$ – see front matter © 2010 Elsevier B.V. All rights reserved.
doi:10.1016/j.cma.2010.01.013

for parallel implementation. A final family of FEM extensions modifies the underlying integral formulations. Examples of this approach are the stabilised FE methods [17–19], the ultra-weak variational formulation [20,21] and multi-scale methods like the discontinuous enrichment [22–24] and discontinuous Galerkin techniques [25,26]. Although all these developments have been instrumental towards alleviating the frequency limitations of the FEM, they share the property that the solution strategies are based on a discretisation of the problem domain which has to conform to the boundary geometry of any inclusion present in the problem domain, like e.g. holes, voids, particles or aggregates. Even though at present many mesh generation algorithms are well established, the creation of high-quality FEM discretisations of domains with an arbitrary number and distribution of defects and inclusions remains a challenging and time-consuming process. Moreover, the main motivation for the development of many of these techniques is to permit relatively rough element sizes to be used up to much higher frequencies at the cost of more complicated, and computationally more expensive, element formulations. When problems with complex multiple inclusion configurations are considered, the gain in computational efficiency of these methods is partly negated by the need to use conforming meshes since in this case the required element sizes are governed by the need to accurately capture the problem geometry rather than by the frequency limitations of the method.

In order to overcome such meshing problems, several special techniques have been developed, which can be divided into two groups. On the one hand there are the techniques which contain special elements of which the problem boundary does not have to coincide with element boundaries. Examples are the extended FEM and the generalised FEM [27–29], in which the finite element approximation fields in elements near the inhomogeneities are enriched (in a partition of unity way) using fields with a strong physical meaning related to the properties of the inhomogeneities [30,31], or techniques which introduce problem-dependent specialist elements in the vicinity of the the inhomogeneity [32–34] while classical finite elements are used to model the remainder of the problem domain. These elements typically use analytical solutions of the governing equation to represent the local behaviour near the inhomogeneity. These approaches have, to the author's knowledge, only been applied successfully to static problems. Due to the mesh resolution requirements resulting from the study of dynamic problems at higher frequencies, the relatively large specialist elements, which typically enclose an entire hole, particle, ..., will couple more and more finite element degrees of freedom to each other, resulting in a significant increase in the bandwidth of the FEM system matrix and a drastic decrease in modelling efficiency. On the other hand, there are techniques which offer elements with a great geometrical flexibility, for example the NURBS-based isogeometric analysis developed by Hughes et al. [35]. However, research on that method has, in the current field of interest, mainly focussed on static problems and free vibrations of structures [36]. A rigorous assessment of the behaviour of this method for the forced response analysis of mid-frequency problems containing multiple inhomogeneities has to the author's knowledge not been performed at present.

In contrast to the previously described FEM and FEM-based techniques, which discretise the entire problem domain into small elements, the BEM [37] is based on a boundary integral formulation of the problem, such that only the boundary of the considered domain has to be discretised. Within the applied boundary elements, some boundary variables are expressed in terms of simple, polynomial shape functions. Enforcement of the boundary conditions results in a small numerical model, as compared to FE models, which can be solved for the nodal values at the discretised boundary. Once these nodal values are known, the field variables inside the domain may be reconstructed by application of the boundary integration formulations in a post processing step. While the use of a boundary discretisation eliminates the problems faced by domain discretisation methods for problems with complex inclusion configurations, the construction of the frequency-dependent, complex, densely populated BE matrices, which includes the integration of singular functions, is very time consuming as compared to the fast assembly of frequency-independent, real valued, sparse FE matrices. In this way, the smaller model size does not necessarily result in an enhanced computational efficiency, so that the practical use of the BEM is also restricted to low-frequency applications [38]. Moreover, when the complexity of the inclusion geometries increases, the number of boundary values grows, resulting in a further lowering of the practical application range of the method.

Apart from the FEM and BEM and all the methods derived from their basic concepts, there is another family of methods, the so called Trefftz methods [39], which distinguish themselves from the FEMs by their choice of shape and weighting functions [40]. Instead of using approximation functions, exact solutions of the governing differential equations are used for the expansion of the field variables. One such Trefftz based method is the Wave Based Method (WBM) [41]. It is a novel numerical prediction method for the analysis of steady-state interior and exterior Helmholtz problems. Since the functions which are applied to expand the dynamic field variables are exact solutions of the governing (system of) Helmholtz equation(s), no residual error is involved with the governing partial differential equation inside the problem domain. However, the functions may violate the boundary conditions. Enforcing the residual boundary errors to zero in a weighted residual scheme yields a small matrix equation. Due to the small model size and the enhanced convergence characteristics of the WBM, it has a superior numerical performance as compared to classical domain discretisation methods. As a result, problems at higher frequencies can be addressed. In the past, the WBM has been successfully applied for the analysis of interior and exterior (vibro-) acoustic problems [42–45] and for the structural dynamic analysis of flat plates [46,47].

One of the important disadvantages of the WBM is the requirement of a division of the problem into convex subdomains to ensure convergence. This requirement necessitates a complex domain splitting for some problem geometries, while other geometries may not be possible at all, e.g. circular holes. Recent work by the authors [48,49] proposes a significantly enhanced multi-level version of the WBM for the analysis of two-dimensional acoustic scattering analysis of a configuration of well separated generally shaped obstacles in an unbounded acoustic medium. In this publication, the basic principles of this approach are further developed into a general modelling framework for the efficient introduction of inclusion configurations in bounded WBM models. Moreover, the applicability of the methodology is extended to encompass any type of dynamic problem governed by one or multiple coupled Helmholtz-type partial differential equations which is illustrated by a numerical verification study of the technique for both steady-state acoustic and elastodynamic problems. The proposed methodology is based on a decomposition of the original (bounded) problem into a single interior subproblem and one or multiple exterior problems. The outer boundary of the interior subproblem matches the outer boundary of the original problem domain while disregarding the inclusions. Each of the exterior problems describes the scattering behaviour of a single inclusion which is embedded in an unbounded homogeneous domain. By modelling each of the subproblems using existing WBM modelling methodologies and applying the superposition principle to the resulting response fields, an efficient and flexible numerical strategy for modelling mid-frequency dynamic multiple inclusion problems is obtained. Concerning the modelling principle, the proposed method is quite similar to the decomposition into two parts using the superposition principle in order to determine the stress concentration factor for an infinite plate with a hole under uniaxial tension, as proposed by Chen in [50]. In that paper, these principles are however only applied to the static analysis of an infinitely extended medium

which contains a single circular hole. The approach presented here is also somewhat similar to the work presented in [51] and [52] on the introduction of heterogeneous substructures in the VTCR methodology [53] for the analysis of mid-frequency vibrations of plates and the work of Stojek [54,55] on the introduction of holes in frameless *T*-elements for the Helmholtz equation. For the VTCR as well as for the *T*-elements, the authors modify the admissible fields which describe the response fields in a set of substructures to *a priori* satisfy the imposed boundary conditions on the boundary of a hole in one of the substructures. In order to determine the modified fields, a set of secondary numerical problems is solved, which, for the VTCR, may involve the need for performing a number of BEM calculations if the hole has a non-circular geometry or if multiple holes are present inside a single substructure. In contrast, the numerical framework presented in this paper is based on adding additional scattering models which are based on existing WBM technology and in which the partitioning of each of the submodels is entirely independent of the other submodels.

The outline of this paper is as follows: Section 2 briefly addresses the general problem setting of a steady-state dynamic problem governed by a system of Helmholtz partial differential equations and describes the WB modelling methodology for two-dimensional unbounded Helmholtz problems. Section 3 illustrates the modelling limitations of the existing WBM approach for multiple inclusion problems and presents the new multi-level concept, which incorporates multiple inclusion modelling in the WB methodology. In Section 4 the new method is applied to the analysis of steady-state acoustic problems, which are governed by a single Helmholtz equation. The general problem setting and most commonly applied types of boundary conditions are discussed and the general multi-level acoustic WBM problem formulations are derived. Furthermore, the method is applied to two numerical verification examples, which both illustrate the feasibility and efficiency of the proposed numerical modelling framework. The subsequent section is devoted to the application of the method to two-dimensional elastodynamic problems, in which the governing equations can be recast into a system of two coupled Helmholtz equations. After detailing the problem setting and the associated multi-level WBM formulations, two numerical verification studies are carried out to analyse the behaviour of the method for problems governed by multiple Helmholtz equations. Finally, Section 6 concludes the paper with general remarks and some possible topics for future research.

2. The Wave Based Method for interior and exterior Helmholtz problems

This section describes the basic principles of the WBM modelling methodology for solving the Helmholtz equation in both bounded and unbounded problem domains. Firstly, a general problem definition is presented. Next, the four basic steps in the general WBM modelling approach are detailed. In the subsequent parts of this section *T*-complete function sets which are used in the WBM for the description of respectively bounded and unbounded Helmholtz problems are given.

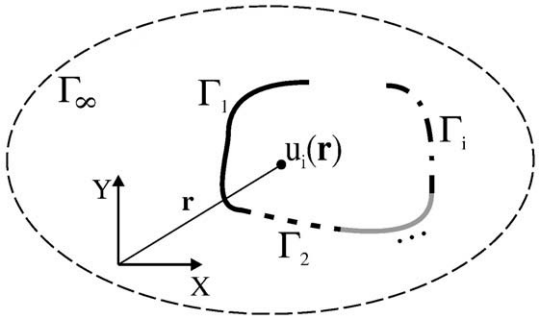

Fig. 1. A general 2D unbounded Helmholtz problem.

2.1. General problem setting

Consider a general two-dimensional interior/exterior steady-state dynamic problem as shown in Fig. 1. The mathematical description of several dynamic phenomena in physics (e.g. structural mechanics, acoustics, electromagnetics, thermal conductivity,...) gives rise to (a coupled system of) the well-known second-order Helmholtz partial differential equation(s):

$$\nabla^2 u_j(\mathbf{r}) + k_j^2 u_j(\mathbf{r}) = \mathcal{F}_j(\mathbf{r}), \mathbf{r} \in \Omega. \tag{1}$$

In this equation $\nabla^2 \bullet = \partial^2 \bullet / \partial x^2 + \partial^2 \bullet / \partial y^2$ is the Laplacian operator, k_j represents the physical wave number and $\mathcal{F}_j(\mathbf{r})$ is a general representation of the non-homogeneous forcing terms which result from the presence of discrete or volumetric sources in the problem setting. The value of the complex physical wave number k_j is determined by the physical properties of the medium inside the problem domain and the excitation frequency ω. In the most general case, the problem boundary Γ consists of 2 parts: the finite part of the boundary, Γ_b, which constitutes the boundary of all the obstacles, and the boundary at infinity, Γ_∞. Based on the available types of commonly applied boundary conditions for each of the specific phenomena described by Eq. (1), the finite boundary can be further divided into a set of non-overlapping parts: $\Gamma_b = \mathbf{U}_i \Gamma_i$, on which a multitude of boundary conditions (of which the Neumann and Dirichlet types are the most widely known) can be applied. These conditions can be written in the following general form:

$$\mathcal{B}_i(u_j(\mathbf{r})) = \overline{\mathcal{B}_i}(\mathbf{r}), \mathbf{r} \in \Gamma_i \tag{2}$$

with $\mathcal{B}_i(\bullet)$ a general boundary differential operator and $\overline{\mathcal{B}_i}(\mathbf{r})$ an imposed boundary field in the case of non-homogeneous boundary conditions. At the boundary at infinity Γ_∞, the enforcement of a non-reflecting boundary condition (like e.g. the well-known Sommerfeld radiation condition [56] applied in acoustics) ensures that the resulting wave field is purely outgoing:

$$\mathcal{B}_\infty(u_j(\mathbf{r})) = 0, \mathbf{r} \in \Gamma_\infty \tag{3}$$

The Helmholtz Equation (1) together with the associated boundary conditions Eq. (2) along Γ_b and Eq. (3) along Γ_∞ define a unique dynamic field $u_j(\mathbf{r})$.

2.2. Basic concepts of the Wave Based Method

The WBM [41] is a numerical modelling method based on an indirect Trefftz approach [39] for the solution of steady-state Helmholtz problems in both bounded and unbounded problem domains. Instead of discretising the entire problem domain (or its boundary) into a large number of small elements and using simple approximating polynomials to describe the dynamic field variables, like in the FEM or BEM, the WBM modelling concept is based on a partitioning of the problem into a limited number of large subdomains. Within each of those subdomains the field variables are expressed as an expansion of wave functions, which intrinsically satisfy the governing equation(s), *in casu* a (set of) Helmholtz-type equation(s) (1). The degrees of freedom are the weighting factors of the wave functions in this expansion. Enforcing the boundary conditions along the problem boundaries and the continuity

conditions on the interfaces between the subdomains using a weighted residual formulation yields a system of linear equations whose solution vector contains the unknown wave function weighting factors.

The general modelling procedure consists of the following steps:

A. Partitioning of the problem domain into subdomains
B. Selection of the wave functions in the field variable expansion
C. Construction of the system of equations through a weighted residual formulation of the boundary and continuity conditions
D. Solution of the system of equations and postprocessing of the dynamic variables

2.2.1. Domain partitioning

When the method is applied to bounded problems, a sufficient condition for the theoretical convergence of the WBM is the convexity of the considered problem domain [41]. In a general Helmholtz problem however, the problem domain may be non-convex requiring the entire problem domain to be partitioned into a number of convex subdomains. If the WBM is applied for unbounded problems, the introduction of an artificial truncation boundary Γ_t restricts the computational domain to a finite region Ω^- [44], much like in the approaches which enable the domain discretisation based modelling strategies to cope with unbounded problems. After this partitioning, the region Ω^- between the truncation boundary and the problem boundary is partitioned into N_Ω non-overlapping, convex subdomains $\Omega^{(\alpha)}$, as is illustrated in Fig. 2. The unbounded region Ω^+ exterior to Γ_t is modelled explicitly as an additional subdomain $\Omega^{(N_\Omega+1)}$, with its own specific type of basis functions. As a result, the combined interior/exteriorproblem domain is partitioned into $N_\Omega+1$ subdomains: $\Omega=\Omega^-\cup\Omega^+=\cup_{\alpha=1}^{N_\Omega+1}\Omega^{(\alpha)}$.

The boundary of each of the subdomains $\Omega^{(\alpha)}$ is denoted as $\partial\Omega^{(\alpha)}$. It consists of a number of mutually exclusive parts (corresponding to each of the types of applied boundary conditions),

$$\partial\Omega^{(\alpha)} = \cup_i \Gamma_i^{(\alpha)}, \quad \alpha = 1,\ldots,N_\Omega+1. \tag{4}$$

The boundary of the unbounded subdomain $\Omega^{(N_\Omega+1)}$ includes the boundary at infinity Γ_∞, along which non-reflecting boundary conditions need to be fulfilled.

In order to enforce the total resulting dynamic fields to be continuous, continuity conditions must be applied at all the interfaces $\Gamma_I^{(\alpha,\beta)}$ between the adjacent subdomains $\Omega^{(\alpha)}$ and $\Omega^{(\beta)}$:

$$\mathcal{B}_I^{(\alpha,\beta)}(u_j^{(\alpha)}(\mathbf{r}), u_j^{(\beta)}(\mathbf{r})) = 0, \mathbf{r}\in\Gamma_I^{(\alpha,\beta)} \tag{5}$$

with $\mathcal{B}_I^{(\alpha,\beta)}(\bullet,\ ^*) = \mathcal{B}_I^{(\alpha)}(\bullet) + \mathcal{B}_I^{(\beta)}(^*)$ a general boundary differential operator expressing the continuity constraints on the fields $\bullet$ and * and their derived quantities and $u_j^{(\alpha)}(\mathbf{r})$ and $u_j^{(\beta)}(\mathbf{r})$ the dynamic fields in both subdomains.

The WBM adopts a direct coupling approach to enforce the coupling condition (5). This implies that the continuity conditions are applied directly on the dynamic quantities of the considered subdomains, without introduction of auxiliary variables. In order for the problem to be well-posed, one continuity condition is imposed on each subdomain for each one of the governing Helmholtz equations.

2.2.2. Field variable expansion

The steady-state dynamic fields $u_j^{(\alpha)}(\mathbf{r})$ in each of the problem subdomains $\Omega^{(\alpha)}$, $\alpha=1\ldots N_\Omega+1$ is approximated by a solution expansion $\hat{u}_j^{(\alpha)}(\mathbf{r})$ in terms of $n_w^{(\alpha)}$ wave functions $\Phi_w^{(\alpha)}$:

$$u_j^{(\alpha)}(\mathbf{r}) \simeq \hat{u}_j^{(\alpha)}(\mathbf{r}) = \sum_{w=1}^{n_w^{(\alpha)}} u_w^{(\alpha)}\Phi_w^{(\alpha)}(\mathbf{r}) + \hat{u}_{p,j}^{(\alpha)}(\mathbf{r}) = \mathbf{\Phi}_\mathbf{w}^{(\alpha)}(\mathbf{r})\,\mathbf{u}_\mathbf{w}^{(\alpha)} + \hat{u}_{p,j}^{(\alpha)}(\mathbf{r}). \tag{6}$$

The wave function contributions $u_w^{(\alpha)}$ are the weighting factors belonging to each of the selected wave functions $\Phi_w^{(\alpha)}$. Together they form the vector of degrees of freedom $\mathbf{u}_\mathbf{w}^{(\alpha)}$. The corresponding *a priori* defined wave functions are collected in the row vector $\mathbf{\Phi}_\mathbf{w}^{(\alpha)}$. The set of all $n_W = \sum_{\alpha=1}^{N_\Omega+1} n_w^{(\alpha)}$ wave function contributions u_w is collected in the column vector $\mathbf{u}_\mathbf{w}$, while the row vector $\mathbf{\Phi}_\mathbf{w}$ contains all n_W wave functions.

Following the indirect Trefftz approach [39], each of the wave functions $\Phi_w^{(\alpha)}(\mathbf{r})$ in the field variable expansion proposed above, exactly satisfies the homogeneous part of the governing Helmholtz Eq. (1). Moreover, in the unbounded region $\Omega^{(N_\Omega+1)}$, these functions are constructed in such a way that they also inherently satisfy the non-reflecting boundary conditions (3) along the boundary at infinity Γ_∞. These conditions do not fully determine the set of basis functions in the expansion and several alternatives are available (e.g. plane waves [20,57,58], Herrera-type function sets [59], ...). Section 2.3 details the different types of wave functions used in the solution expansions for both bounded and unbounded WBM subdomains governed by the Helmholtz equation.

$\hat{u}_{pj}^{(\alpha)}$ represents a particular solution resulting from the combined source terms $\mathcal{F}_j(\mathbf{r})$ in the right hand side of the inhomogeneous Helmholtz Eq. (1). The nature of these functions is determined by the physical interpretation of $\mathcal{F}_j(\mathbf{r})$ as a superposition of distinct (correlated or uncorrelated) problem-specific dynamic sources (e.g. acoustic volume velocity sources, structural forces,...) and will be described in Sections 4 and 5 which detail the application of the WBM to specific problem types. Usually these particular solution functions take the form of the dynamic fields generated by the sources in an infinitely extended homogeneous medium.

2.2.3. Evaluation of boundary and interface conditions

With the use of the proposed solution expansion Eq. (6), the Helmholtz Eq. (1) and the radiation condition (3) are always exactly satisfied, irrespective of the values of the unknown wave function contributions u_w. These contributions are entirely determined by the imposed boundary and continuity conditions. Both the boundary and the continuity conditions are defined at an infinite number of boundary positions. Since only finite sized prediction models are amenable to numerical implementation, the boundary and the continuity conditions are, for each subdomain, transformed into a weighted residual formulation. In this formulation, the residual errors on the boundary and continuity

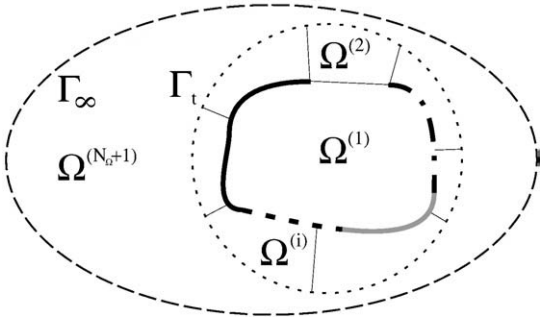

Fig. 2. A WB partitioning of the 2D unbounded problem.

conditions are orthogonalised with respect to a set of weighting functions $\tilde{t}^{(\alpha)}$:

$$\sum_i \int_{\Gamma_i^{(\alpha)}} \tilde{t}_i^{(\alpha)}(\mathbf{r})\left(\mathcal{B}_i(\hat{u}^{(\alpha)}(\mathbf{r})) - \overline{\mathcal{B}}_i(\mathbf{r})\right) d\Gamma + \sum_{\beta=1,\beta\neq\alpha}^{N_\Omega+1} \int_{\Gamma_I^{(\alpha,\beta)}} \tilde{t}_I^{(\alpha)}(\mathbf{r}) \mathcal{B}_I^{(\alpha,\beta)}(\hat{u}^{(\alpha)}(\mathbf{r}), \hat{u}^{(\beta)}(\mathbf{r})) d\Gamma = 0, \quad \alpha = 1 \ldots N_\Omega + 1. \tag{7}$$

In general, the weighting functions $\tilde{t}_\bullet^{(\alpha)}(\mathbf{r})$ for each type of boundary and continuity condition can be interpreted as physical quantities derived from an underlying weighting function $t^{(\alpha)}(\mathbf{r})$. The definition of these quantities is determined based on a variational analysis of the problem being solved [60]:

$$\tilde{t}_\bullet^{(\alpha)}(\mathbf{r}) = \mathcal{D}_\bullet\left(t^{(\alpha)}(\mathbf{r})\right) \tag{8}$$

with $\mathcal{D}_\bullet(*)$ a problem- and condition-specific differential operator. Like in the Galerkin weighting procedure used in the FEM, the weighting functions $t^{(\alpha)}$ are expanded in terms of the same set of basis functions used in the dynamic field variable expansions:

$$\tilde{t}_\bullet^{(\alpha)}(\mathbf{r}) = \mathcal{D}_\bullet\left(\sum_{w=1}^{n_w^{(\alpha)}} t_w^{(\alpha)} \Phi_w^{(\alpha)}(\mathbf{r})\right) = \mathcal{D}_\bullet\left(\boldsymbol{\Phi}_{\mathbf{w}}^{(\alpha)}(\mathbf{r})\right) \mathbf{t}_w^{(\alpha)}. \tag{9}$$

From here onwards, the position dependency of the vectors is omitted in the notations to enhance the readability.

Substitution of the field variable expansion (6) and the weighting function expansion (9) into the weighted residual formulation (7) yields an algebraic equation linking the unknown wave function contributions for subdomain $\Omega^{(\alpha)}$ to those of the adjacent subdomains. Construction of a similar set of algebraic equations for all subdomains $\Omega^{(\alpha)}$, $\alpha = 1 \ldots N_\Omega + 1$ and enforcing that these should hold for any arbitrary weighting function results in a fully populated, complex and generally non-symmetric system of equations consisting of n_W algebraic equations governing the n_W unknown wave function contribution factors u_w:

$$\begin{bmatrix} \boldsymbol{A}_{aa}^{(1,1)} & \boldsymbol{C}_{aa}^{(1,2)} & \cdots & \boldsymbol{C}_{aa}^{(1,N_\Omega+1)} \\ \boldsymbol{C}_{aa}^{(2,1)} & \boldsymbol{A}_{aa}^{(2,2)} & \cdots & \boldsymbol{C}_{aa}^{(2,N_\Omega+1)} \\ \vdots & \vdots & \ddots & \vdots \\ \boldsymbol{C}_{aa}^{(N_\Omega+1,1)} & \boldsymbol{C}_{aa}^{(N_\Omega+1,2)} & \cdots & \boldsymbol{A}_{aa}^{(N_\Omega+1,N_\Omega+1)} \end{bmatrix} \cdot \begin{bmatrix} \mathbf{u}_{\mathbf{w}}^{(1)} \\ \mathbf{u}_{\mathbf{w}}^{(2)} \\ \vdots \\ \mathbf{u}_{\mathbf{w}}^{(N_\Omega+1)} \end{bmatrix} = \begin{bmatrix} \sum_\beta \mathbf{f}_{\mathbf{a}}^{(1,\beta)} \\ \sum_\beta \mathbf{f}_{\mathbf{a}}^{(2,\beta)} \\ \vdots \\ \sum_\beta \mathbf{f}_{\mathbf{a}}^{(N_\Omega+1,\beta)} \end{bmatrix} \tag{10}$$

The underlying integral formulations for the system matrices $A_{aa}^{(\bullet,\bullet)}$, coupling matrices $C_{aa}^{(\bullet,\bullet)}$ and loading vectors $\mathbf{f}_{\mathbf{a}}^{(\bullet)}$ can be written as:

$$\begin{aligned} \boldsymbol{A}_{\boldsymbol{aa}}^{(\boldsymbol{\alpha},\boldsymbol{\alpha})} &= \sum_i \int_{\Gamma_i} \mathcal{D}_i\left(\boldsymbol{\Phi}_{\mathbf{w}}^{(\alpha)}\right)^T \mathcal{B}_i\left(\boldsymbol{\Phi}_{\mathbf{w}}^{(\alpha)}\right) d\Gamma \\ &\quad + \sum_{\beta=1,\beta\neq\alpha}^{N_\Omega+1} \int_{\Gamma_I^{(\alpha,\beta)}} \mathcal{D}_I\left(\boldsymbol{\Phi}_{\mathbf{w}}^{(\alpha)}\right)^T \mathcal{B}_I^{(\alpha)}\left(\boldsymbol{\Phi}_{\mathbf{w}}^{(\alpha)}\right) d\Gamma \\ \boldsymbol{C}_{\boldsymbol{aa}}^{(\boldsymbol{\alpha},\boldsymbol{\beta})} &= \int_{\Gamma_I^{(\alpha,\beta)}} \mathcal{D}_I\left(\boldsymbol{\Phi}_{\mathbf{w}}^{(\alpha)}\right)^T \mathcal{B}_I^{(\beta)}\left(\boldsymbol{\Phi}_{\mathbf{w}}^{(\beta)}\right) d\Gamma \\ \boldsymbol{f}_{\boldsymbol{a}}^{(\boldsymbol{\alpha},\boldsymbol{\alpha})} &= -\sum_i \int_{\Gamma_i} \mathcal{D}_i\left(\boldsymbol{\Phi}_{\mathbf{w}}^{(\alpha)}\right)^T \left(\overline{\mathcal{B}}_i - \mathcal{B}_i\left(\hat{u}_p^{(\alpha)}\right)\right)) d\Gamma \\ &\quad + \sum_{\beta=1,\beta\neq\alpha}^{N_\Omega+1} \int_{\Gamma_I^{(\alpha,\beta)}} \mathcal{D}_I\left(\boldsymbol{\Phi}_{\mathbf{w}}^{(\alpha)}\right)^T \mathcal{B}_I^{(\alpha)}\left(\hat{u}_p^{(\alpha)}\right) d\Gamma \\ \boldsymbol{f}_{\boldsymbol{a}}^{(\boldsymbol{\alpha},\boldsymbol{\beta})} &= -\int_{\Gamma_I^{(\alpha,\beta)}} \mathcal{D}_I\left(\boldsymbol{\Phi}_{\mathbf{w}}^{(\alpha)}\right)^T \mathcal{B}_I^{(\beta)}\left(\hat{u}_p^{(\beta)}\right) d\Gamma \end{aligned} \tag{11}$$

The calculation of the matrix coefficients involves integrations of highly oscillatory functions. Because the WBM, like any Trefftz based method, yields ill-conditioned system matrices [61,62], the numerical integrations must be performed carefully, making sure that a sufficiently high accuracy in determining the matrix coefficients is obtained. Applying a classical Gauss-Legendre numerical integration scheme [63] with a frequency-dependent number of quadrature points (typically a constant number of integration points per oscillatory wavelength of the integrand [60,64,65]) results in an efficient evaluation of the system matrix while avoiding convergence problems related to integration errors.

2.2.4. Solution of the system of equations and postprocessing

After selecting a converging set of wave functions and constructing the WB model, the third step in the WB modelling process is the solution of the WB matrix Eq. (10) for the n_W wave function contribution factors u_w. As mentioned in the discussion of the WBM matrices, the numerical conditioning of the WBM models tends to be poor. However, Desmet [41] shows that nonetheless an accurate numerical solution can be obtained using standard direct solution algorithms because the matrices fulfill the so-called Picard conditions [66,67].

The final step is a back substitution of the resulting wave function contribution factors into the field variable expansions (6), yielding an approximation $\hat{u}_j(\mathbf{r})$ of the dynamic field variables. Derived variables, such as acoustic velocities, dynamic structural stresses and acoustic and structural intensities, can be easily obtained by applying the corresponding differential operators to the proposed wave function set $\boldsymbol{\Phi}_{\mathbf{w}}$ and combining these quantities with the calculated contribution factors $\mathbf{u}_{\mathbf{w}}$.

2.3. Wave functions expansions for interior and exterior Helmholtz problems

The general field variable expansion (6) applies to every computational technique which is based on the Trefftz principle. The choice of a specific class of basis functions in these methods is crucial, since they determine to a great extent the stability and the convergence of the numerical scheme. In this section, a set of wave functions $\Phi_w^{(\alpha)}$ is proposed for both interior and exterior subdomains governed by the Helmholtz Eq. (1) which has proven to result in a stable and convergent modelling approach.

2.3.1. Wave functions for a bounded subdomain $\Omega^{(\alpha)}$

Each wave function $\Phi_w^{(\alpha)}(\mathbf{r})$ exactly satisfies the homogeneous Helmholtz Eq. (1). For 2D bounded subdomains, two types of wave functions which govern the homogeneous part of the Helmholtz equation are distinguished, the *r*- and the *s*-set:

$$\sum_{w=1}^{n_w^{(\alpha)}} u_w^{(\alpha)} \Phi_w^{(\alpha)}(\mathbf{r}) = \sum_{w_r=1}^{n_{w_r}^{(\alpha)}} u_{w_r}^{(\alpha)} \Phi_{w_r}^{(\alpha)}(\mathbf{r}) + \sum_{w_s=1}^{n_{w_s}^{(\alpha)}} u_{w_s}^{(\alpha)} \Phi_{w_s}^{(\alpha)}(\mathbf{r}), \tag{12}$$

with $n_w^{(\alpha)} = n_{w_r}^{(\alpha)} + n_{w_s}^{(\alpha)}$. These wave functions exhibit harmonic behaviour along one of the local coordinate directions and behave like a complex exponential function along the other:

$$\Phi_w^{(\alpha)}(\mathbf{r}(x,y)) = \begin{cases} \Phi_{w_r}^{(\alpha)}(x,y) = \left\{sin(k_{xw_r}^{(\alpha)} x), cos(k_{xw_r}^{(\alpha)} x)\right\} e^{-jk_{yw_r}^{(\alpha)} y} \\ \Phi_{w_s}^{(\alpha)}(x,y) = e^{-jk_{xw_s}^{(\alpha)} x}\left\{sin(k_{yw_s}^{(\alpha)} y), cos(k_{yw_s}^{(\alpha)} y)\right\} \end{cases} \tag{13}$$

where $\{f(x, y), g(x, y)\}h(x, y)$ indicates the definition of two independent basis functions $f(x, y).h(x, y)$ and $g(x, y).h(x, y)$.

The only requirement for the wave function Eq. (13) to be exact solutions of Eq. (1) is

$$\left(k_{xw_r}^{(\alpha)}\right)^2 + \left(k_{yw_r}^{(\alpha)}\right)^2 = \left(k_{xw_s}^{(\alpha)}\right)^2 + \left(k_{yw_s}^{(\alpha)}\right)^2 = k_j^2. \tag{14}$$

As a result, an infinite number of wave function Eq. (13) can be defined for expansion (12). Desmet [41] proposes to select the following wave number components

$$\left(k_{xw_r}^{(\alpha)}, k_{yw_r}^{(\alpha)}\right) = \left(\frac{w_1^{(\alpha)}\pi}{L_x^{(\alpha)}}, \pm\sqrt{k_j^2 - \left(k_{xw_r}^{(\alpha)}\right)^2}\right), \quad w_1^{(\alpha)} = 0,1,2,\ldots \tag{15}$$

$$\left(k_{xw_s}^{(\alpha)}, k_{yw_s}^{(\alpha)}\right) = \left(\pm\sqrt{k_j^2 - \left(k_{yw_s}^{(\alpha)}\right)^2}, \frac{w_2^{(\alpha)}\pi}{L_y^{(\alpha)}}\right), \quad w_2^{(\alpha)} = 0,1,2,\ldots \tag{16}$$

The dimensions $L_x^{(\alpha)}$ and $L_y^{(\alpha)}$ represent the dimensions of the (preferably smallest) bounding rectangle, circumscribing the considered subdomain $\Omega^{(\alpha)}$, which is called the associated 'bounding box' BB_α. The proposed wave function set satisfies the Helmholtz equation in any Cartesian coordinate system. In order to uniquely define these functions, a local (x_α, y_α) coordinate system is associated to the considered bounded subdomain $\Omega^{(\alpha)}$. The origin of this coordinate system is placed in the corner of BB_α and both axes are placed along the edges of the rectangle, such that all points inside the subdomain have positive local coordinate values.

In order to apply the WBM in a numerical scheme, the expansion of wave functions must be truncated to a finite set. The adopted truncation rule is frequency dependent and selects the upper limits $w_{\{1,2\},max}^{(\alpha)}$ for the integers $w_1^{(\alpha)}$ and $w_2^{(\alpha)}$ in Eqs. (15) and (16) such that the corresponding wave number k_{max} of the highest oscillating wave function is higher than a user-defined truncation parameter T times the physical wavenumber k_j of the considered problem:

$$k_{max} = \frac{w_\bullet^{(\alpha)}\pi}{L_\bullet^{(\alpha)}} \geq Tk_j. \tag{17}$$

The physical wavenumber k_j corresponds to the largest physical wavenumber of the different subdomains so that the approximation fields in adjacent subdomains exhibit similar spatial variations along the common interface. The number of included wave functions results from the specification of T and increases approximately linearly with the excitation frequency. Typical values for the truncation parameter are $T = 1\ldots6$.

2.3.2. Wave functions for an unbounded subdomain

The wave functions for the unbounded domain $\Omega^{(N_\Omega+1)}$ are chosen to implicitly comply with not only the Helmholtz Eq. (1), but also with the non-reflecting condition (3) at Γ_∞. This removes the need to explicitly impose a radiation condition, similar to the Green's functions applied in the BEM. Herrera [59] shows that the following expansion yields a complete set of basis functions for a homogeneous Neumann problem exterior to an infinitely long circular cylinder with radius R:

$$\sum_{w=1}^{n_w^{(N_\Omega+1)}} u_w^{(N_\Omega+1)}\Phi_w^{(N_\Omega+1)}(\mathbf{r}) = u_0^{(N_\Omega+1)}H_0^{(2)}(k_j r) + \sum_{w=1}^{N}\left(u_{w_c}^{(N_\Omega+1)}H_w^{(2)}(k_j r)cos(w\theta) + u_{w_s}^{(N_\Omega+1)}H_w^{(2)}(k_j r)sin(w\theta)\right), \tag{18}$$

with r and θ polar coordinates, N the number of circumferential orders in the solution expansion ($n_w^{(N_\Omega+1)} = 2N+1$) and $H_w^{(2)}(\bullet)$ the w-th order Hankel function of the second kind. The contributions u_0, u_{w_c} and u_{w_s} are determined by the imposed velocity distribution along the circumference of the cylinder. From this expansion, the following set of wave functions for unbounded domains is derived:

$$\Phi_w^{(N_\Omega+1)}(\mathbf{r}(r,\theta)) = \begin{cases} \Phi_{w_c}^{(N_\Omega+1)}(r,\theta) = H_w^{(2)}(k_j r)cos(w\theta), & w = 0,1,2,\ldots \\ \Phi_{w_s}^{(N_\Omega+1)}(r,\theta) = H_w^{(2)}(k_j r)sin(w\theta), & w = 1,2,3,\ldots \end{cases}. \tag{19}$$

In order to uniquely define this set of wave functions, they are defined in a local polar coordinate system (r,θ), which is located in the center of the circular truncation boundary.

The number of wave functions used in the exterior wave function expansions is determined by applying a truncation rule similar to Eq. (17) for the bounded domains to the circumferential resolution of $\Phi_w^{(N_\Omega+1)}(\mathbf{r}(r,\theta))$:

$$k_{max} = \frac{w_{max}}{2R} \geq Tk_j. \tag{20}$$

3. A Trefftz-based numerical framework for multiple inclusion modelling in Helmholtz problems

The WBM approach described in Section 2 has proven to be an efficient modelling technique for the study of low- and mid-frequency two-dimensional interior and scattering problems governed by the Helmholtz equation [45]. The applied partitioning approach and the underlying geometrical convergence requirements impose however severe limitations to the applicability of the method when an interior problem with multiple inclusions is considered. This section discusses these limitations in more detail and proposes a solution in the form of a novel multi-level modelling concept. The basic concepts of this approach are similar to the multi-level modelling framework proposed by the authors in [48,49] to overcome the limitations of the WBM for multiple scattering problems in unbounded domains with many well separated scatterers. The approach presented here is based on an alternative problem partitioning strategy and the application of the superposition principle to the wave fields in two derived Helmholtz problems. On the one hand, a bounded WBM model is built for the exterior boundary of the considered problem, while the inclusions are neglected. On the other hand, an unbounded WBM model is constructed which describes the scattering behaviour of the inclusion(s) in an infinite homogeneous medium. Moreover, if the inclusion configuration consists of multiple well separated objects, the framework presented here can be combined with the approach for multiple scattering problems in [49] into a general modelling framework for the efficient analysis of interior Helmholtz problems with complex inclusion configurations.

3.1. Bounded WBM modelling limitations

The WBM has shown to be efficient in modelling 2D interior Helmholtz problems [44]. However, when the problem geometry consists of a cavity with moderately complex exterior boundary which contains one or multiple inclusions, the methods efficiency tends to deteriorate. This decrease in efficiency is mainly caused by the geometrical convergence requirements imposed by the wave function expansion for interior domains (13), as is illustrated in Fig. 3. When the problem domain consists of a convex cavity containing a simple square hole, a domain partitioning into 4 WBM subdomains as shown in Fig. 3 (b) is needed to ensure the convergence of the model. Moreover, a partitioning into 4 domains results in at least two domains with boundaries along which the imposed boundary conditions are discontinuous. Hence, the convergence rate of the resulting WBM model will be suboptimal since many continuous wave functions are needed in order to accurately describe the jumps in the subdomain boundary variables. As a

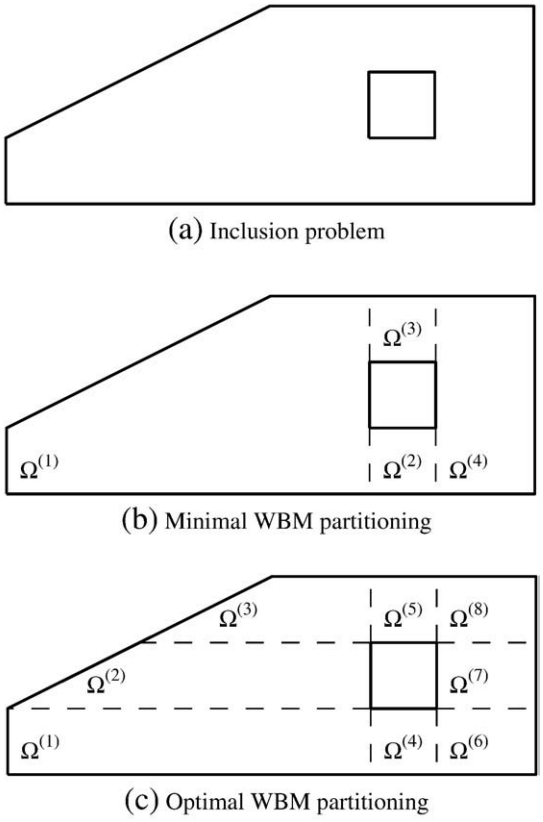

Fig. 3. Illustration of the bounded WBM modelling limitations.

result, the partitioning in 8 domains as shown in Fig. 3(c) is preferred in order to retain an optimal practical convergence rate of the method [45].

The simple example above clearly illustrates the limitations of the WBM methodology. Since the classical WBM model needs to take into account all the inclusions at once when describing the problem geometry, a complex partitioning of the interior region is often needed in order to meet the theoretical convergence requirements. This increase in subdomains is disadvantageous for the convergence rate of the method, since it introduces many additional subdomain interfaces along which continuity conditions need to be enforced. Moreover, some very common geometrical features cannot be dealt with at all. A typical example of this is the study of the dynamic behaviour of a two-dimensional convex cavity which contains two or more circular obstacles. Since the region between two holes or between a hole and the exterior boundary needs to be partitioned into convex subdomains, only an approximate, linearised representation of the circular edge can be used to construct a convergent WBM model. The resulting model is only a crude geometrical approximation of the actual problem and has the additional disadvantage of being inefficient since a reasonable representation accuracy of the circle requires many convex subdomains surrounding it.

3.2. Inclusion problem decomposition

To remedy the modelling limitations for multiple scattering problems in an unbounded acoustic domain, the concept of multi-level WBM scattering modelling was introduced in [48,49]. The main idea of the multi-level WBM approach is to consider the different scatterers in the problem as n_λ different 'levels' of the problem. In every level, the scattering of one particular object is studied by means of a classical unbounded WBM model, associated to that level of the problem. The total solution field is written as a combination of the all wave functions belonging to each of the levels.

The limitations of the WBM for the analysis of interior problems with multiple inclusions can be resolved by extending the unbounded multi-level scattering formalism to a combined bounded–unbounded multi-level formalism. This is done by decomposing the considered problem into two related Helmholtz problems, see Fig. 4 for the case of a single inclusion. The first 'level' describes the interior dynamic behaviour of the cavity delimited only by the exterior boundary of the original problem (bottom-right in Fig. 4). The second level considers the multiple scattering behaviour of the inclusion configuration in an infinite homogeneous medium (top-right in Fig. 4). When a configuration of multiple inclusions is analysed, the latter is delimited by a composite truncation boundary Γ_t' which consists of a collection of circles, each of which encloses one of the inclusions. The multiple scattering problem can then be dealt with using the already developed WBM multiple scattering

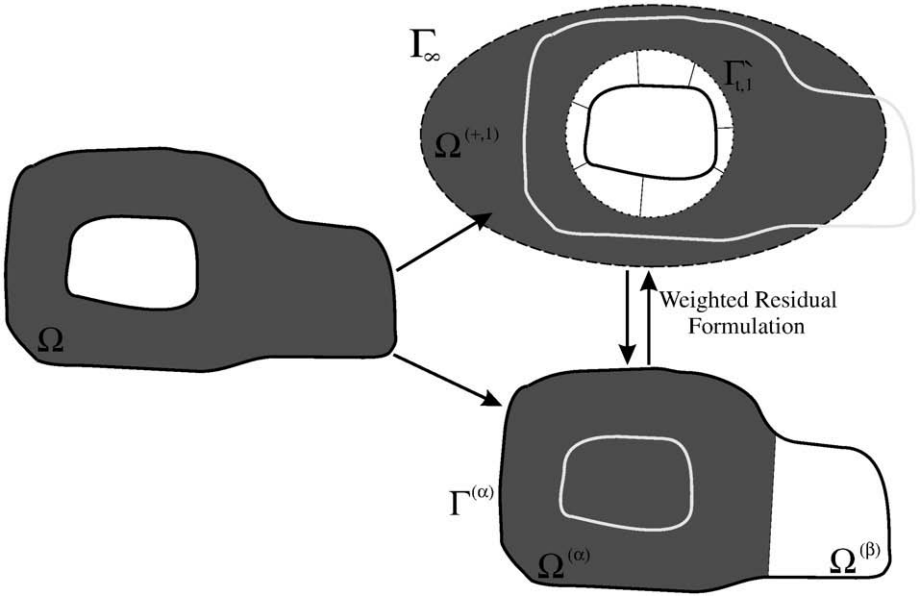

Fig. 4. General single inclusion problem.

modelling [48,49]. Since the exterior solution field in the second 'level' can no longer be expanded in terms of a single series of exact solutions of the Helmholtz equation because there exists no single coordinate system in which the Helmholtz operator is separable in the region exterior to Γ'_t, the multi-level WBM scattering approach divides the scattering level further into several levels, each containing one single scattering object.

A more detailed derivation of this approach starts by considering the general single inclusion problem given in Fig. 4. In a first step, the inclusion is enclosed by a close-fitting circular truncation boundary $\Gamma'_{t,1}$ and a local polar coordinate system (r_1, θ_1) is defined in the center c_1 of this circle. The exterior region outside of this truncation geometry is defined as $\Omega^{+,1}$. At the same time, the entire interior domain inside the outer problem boundary is partitioned into N_Ω convex bounded WBM subdomains. For the purpose of this derivation, it is assumed that the entire truncation geometry $\Gamma'_{t,1}$ is located inside a single subdomain $\Omega^{(\alpha)}$ of the bounded domain partitioning. Note however that this assumption is solely made for ease of notation and should not be considered as a supplementary constraint upon the partitioning of the simplified bounded problem. A local Cartesian coordinate system (x_α, y_α) is defined in one of the corners c_α of the bounding box associated to $\Omega^{(\alpha)}$. Based on these definitions, the solution field $u_i^{(\alpha')}(\mathbf{r})$ in the region of interest $\Omega^{(\alpha')}$, in which both the bounded subdomain $\Omega^{(\alpha)}$ and unbounded region $\Omega^{+,1}$ overlap, is now decomposed into a bounded wave field $u_j^{(\alpha)}$ and an unbounded wave field $u_j^{(\alpha,1)}$, which both solve the governing Helmholtz equation(s) and the latter of which also inherently satisfies the non-reflecting boundary conditions imposed at Γ_∞:

$$\nabla^2 u_j^{(\alpha)}(x_\alpha, y_\alpha) + k_j^2 u_j^{(\alpha)}(x_\alpha, y_\alpha) = 0, \quad (x_\alpha, y_\alpha) \in \Omega^{(\alpha)} \tag{21}$$

and

$$\nabla^2 u_j^{(\alpha,1)}(r_1, \theta_1) + k_j^2 u_j^{(\alpha,1)}(r_1, \theta_1) = 0, \quad (r_1, \theta_1) \in \Omega^{+,1} \tag{22}$$

$$\mathcal{B}_\infty\left(u_j^{(\alpha,1)}(r_1, \theta_1)\right) = 0. \tag{23}$$

Both fields are constructed independently of each other. Field $u_j^{(\alpha,1)}$ is entirely determined by the conditions which are imposed along the truncation circle $\Gamma'_{t,1}$ and field $u_j^{(a)}$ only depends on the conditions along $\Gamma^{(\alpha)}$. To solve these problems, the WBM for bounded and unbounded problems as described in Section 2 can be applied. This results in two independent wave function expansions for each of the superimposed wave fields:

$$\Phi_w^{(\alpha)}(\mathbf{r}(x_\alpha, y_\alpha)) = \begin{cases} \Phi_{w_r}^{(\alpha)}(x_\alpha, y_\alpha) = \left\{sin\left(k_{xw_r}^{(\alpha)} x_\alpha\right), cos\left(k_{xw_r}^{(\alpha)} x_\alpha\right)\right\} e^{-jk_{yw_r}^{(\alpha)} y_\alpha} \\ \Phi_{w_s}^{(\alpha)}(x_\alpha, y_\alpha) = e^{-jk_{xw_s}^{(\alpha)} x_\alpha}\left\{sin\left(k_{yw_s}^{(\alpha)} y_\alpha\right), cos\left(k_{yw_s}^{(\alpha)} y_\alpha\right)\right\} \end{cases}. \tag{24}$$

and

$$\Phi_w^{(\alpha,1)}(r_1, \theta_1) = \begin{cases} \Phi_{w_c}^{(\alpha,1)}(r_1, \theta_1) = H_w^{(2)}\left(k_j r_1\right) cos(w\theta_1) \\ \Phi_{w_s}^{(\alpha,1)}(r_1, \theta_1) = H_w^{(2)}\left(k_j r_1\right) sin(w\theta_1) \end{cases}. \tag{25}$$

Finally, the wave field of interest $u_j^{(\alpha')}$ is constructed by combining the unbounded wave field $u_j^{(\alpha,1)}$ and the bounded field $u_j^{(\alpha)}$:

$$u_j^{(\alpha')}(\mathbf{r}) = u_j^{(\alpha,1)}(r_1, \theta_1) + u_j^{(\alpha)}(x_\alpha, y_\alpha), \quad (\mathbf{r}) \in \Omega^{(\alpha')}. \tag{26}$$

In the more general case where multiple inclusions may be present inside a single bounded subdomain, the scattering model of the inclusion configuration applied in the derivation above may be replaced by an equivalent decomposition into multiple single scattering problems like in the multiple scattering WBM in [49]. This results in applying the superposition principle to a single bounded wave function set and multiple sets of unbounded wave functions, each linked to a single inclusion in the configuration. Moreover, in the case of multiple inclusions, it becomes likely that not all inclusions are located within a single bounded subdomain. If this is the case, only the outgoing wave fields associated to inclusions which are located within bounded subdomain $\Omega^{(\alpha)}$ are superimposed to the interior field $u_j^{(\alpha)}$. The influence of the inclusion(s) is propagated to the remaining subdomains in the problem partitioning by applying the continuity condition (5) to the decomposed wave field in $\Omega^{(\alpha')}$ and the fields in the adjacent subdomains. If the truncation circle of a single inclusion would intersect an interface between two subdomains $\Omega^{(\alpha)}$ and $\Omega^{(\beta)}$ in the bounded problem partitioning, the superposition principle is applied to the associated exterior wave field and both bounded fields $u_j^{(\alpha)}$ and $u_j^{(\beta)}$.

3.3. Multi-level field variable expansion and weighted residual formulation

Consider a general bounded Helmholtz problem with multiple inclusions. The general inclusion problem configuration is firstly decomposed into two subproblems. One subproblem studies the dynamic behaviour of the interior problem defined by the outer problem boundary while disregarding the presence of the inclusions. Meanwhile the complementary subproblem describes the response of the inclusion configuration embedded in an infinitely extended homogeneous domain. The former problem is partitioned into a number of bounded subdomains, in which each bounded subdomain $\Omega^{(\alpha)}$ contains $n_\lambda^{(\alpha)}$ inclusions for each of which a unique truncation circle $\Gamma'^{(\alpha)}_{t,L_i}$ is introduced in the latter submodel. Each of the truncation circles $\Gamma'^{(\alpha)}_{t,L_i}$ defines a so-called 'level' L_i in the multiple inclusion model. In each of these levels, the unbounded (outgoing) wave-field $u_j^{(\alpha,L_i)}$ can be described using a wave function expansion of type Eq. (25). By matching all these expansions and the bounded wave function expansion $u_j^{(\alpha)}$ belonging to the subdomain in which the inclusions reside, the dynamic field $u_j^{(\alpha')}$ in the overlapping region $\Omega^{(\alpha')}$ of the total problem will be described as a summation of the fields present in each level:

$$\begin{aligned} u_j^{(\alpha')} &= \mathbf{\Phi}^{(\alpha)} \cdot \mathbf{u}_\mathbf{w}^{(\alpha)} + \sum_{L_i=1}^{n_\lambda^{(\alpha)}} \mathbf{\Phi}^{(\alpha,L_i)} \cdot \mathbf{u}_\mathbf{w}^{(\alpha,L_i)} \\ &= \left[\mathbf{\Phi}^{(\alpha)} \mathbf{\Phi}^{(\alpha,L_1)} \ldots \mathbf{\Phi}^{(\alpha,L_{n_\lambda^{(\alpha)}})}\right] \cdot \begin{bmatrix} \mathbf{u}_\mathbf{w}^{(\alpha)} \\ \mathbf{u}_\mathbf{w}^{(\alpha,L_1)} \\ \vdots \\ \mathbf{u}_\mathbf{w}^{(\alpha,L_{n_\lambda^{(\alpha)}})} \end{bmatrix}. \end{aligned} \tag{27}$$

The modelling principle proposed here is illustrated in Fig. 5 for a convex bounded Helmholtz problem which contains two circular inclusions. In order to model this problem, one bounded subdomain $\Omega^{(\alpha)}$ and two unbounded truncation circles $\Gamma'^{(\alpha)}_{t,1}$ and $\Gamma'^{(\alpha)}_{t,2}$ which coincide with the inclusions are introduced. Applying the multi-level modelling idea, the solution field in the region $\Omega^{(\alpha')}$, which is shaded grey in the figure, is written a superposition of one set of bounded wave functions $\Phi_w^{(\alpha)}$ and two sets of unbounded wave-fields $\Phi_w^{(\alpha,1)}$ and $\Phi_w^{(\alpha,2)}$. The nature of these three approximation bases is graphically illustrated in the figures at the bottom of Fig. 5.

Now that the function set is defined, the wave model for this domain can be constructed by enforcing the boundary and continuity conditions through the application of a weighted residual formulation. This formulation is analogue to Eq. (7), but the residuals are now expressed in terms of the new, composite wave function set. The

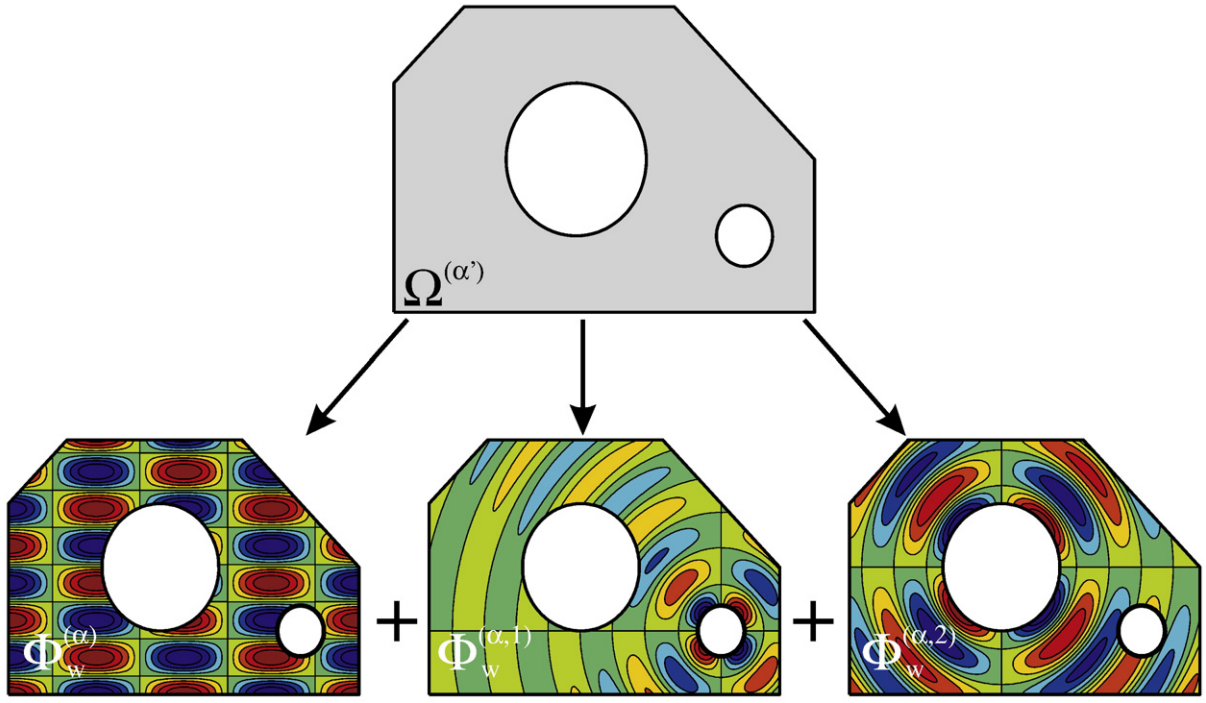

Fig. 5. Illustration of the field variable approximation function superposition in the multi-level modelling approach.

continuity conditions in this formulation can be used to couple the multi-level inclusion wave set with other bounded domains or even an unbounded WBM model, in the same way as a coupling would be set up between conventional unbounded and bounded wave domains. The bounded region inside each of the truncation circles can then be modelled using the conventional wave based domain division techniques and function sets or could even be modelled using multi-level domains with their own specific composite basis function sets. The weighted residual formulation is written as:

$$\sum_{\alpha=1}^{N_\Omega}\Bigg[\sum_i\Bigg(\int_{\Gamma_i^{(\alpha')}}\mathcal{D}_i\left(t^{(\alpha')}\right)\mathcal{B}_i\left(u^{(\alpha)}\right)d\Gamma-\int_{\Gamma_i^{(\alpha')}}\mathcal{D}_i\left(t^{(\alpha')}\right)\overline{\mathcal{B}}_i d\Gamma + \sum_{L_i=1}^{n_\Lambda^{(\alpha)}}\int\Gamma_i^{(\alpha')}\mathcal{D}_i\left(t^{(\alpha')}\right)\mathcal{B}_i\left(u^{(\alpha,L_i)}\right)d\Gamma\Bigg) + \sum_{\beta=1,\beta\neq\alpha}^{N_\Omega}\Bigg(\int_{\Gamma_I^{(\alpha'\beta')}}\mathcal{D}_I\left(t^{(\alpha')}\right)\mathcal{B}_I^{(\alpha)}\left(u^{(\alpha)}\right)d\Gamma + \int_{\Gamma_I^{(\alpha'\beta')}}\mathcal{D}_I\left(t^{(\alpha')}\right)\mathcal{B}_I^{(\beta)}\left(u^{(\beta)}\right)d\Gamma + \sum_{L_i=1}^{n_\Lambda^{(\alpha)}}\int_{\Gamma_I^{(\alpha'\beta')}}\mathcal{D}_I\left(t^{(\alpha')}\right)\mathcal{B}_I^{(\alpha)}\left(u^{(\alpha,L_i)}\right)d\Gamma + \sum_{L_i=1}^{n_\Lambda^{(\beta)}}\int_{\Gamma_I^{(\alpha'\beta')}}\mathcal{D}_I\left(t^{(\alpha')}\right)\mathcal{B}_I^{(\beta)}\left(u^{(\beta,L_i)}\right)d\Gamma\Bigg)\Bigg]=0 \tag{28}$$

with $\Gamma_i^{(\alpha')}=\Gamma^{(\alpha')}\cap\Gamma_i$ and $\Gamma_I^{(\alpha',\beta')}$ the overlapping part of the boundary of domains $\Omega^{(\alpha')}$ and $\Omega^{(\beta')}$. The latter can either be interface surfaces between two bounded domains or the interface between a bounded subdomain and the truncation circle $\Gamma'^{(\alpha)}_{t,i}$ around an inclusion in the case of non-circular inclusions.

If the test functions $t^{(\alpha')}(\mathbf{r})$ in Eq. (28) are random functions, then the residual errors on the boundary and continuity conditions are forced to zero in an integral sense. To obtain a numerical model which can be solved, the test functions related to subdomain $\Omega^{(\alpha')}$ are expanded in terms of a set of basis functions $\Psi_w^{(\alpha')}(\mathbf{r})$:

$$t^{(\alpha')}(\mathbf{r})=\sum_{w=1}^{n_w^{(\alpha')}}t_w^{(\alpha')}\Psi_w^{(\alpha')}(\mathbf{r})=\Psi^{(\alpha')}(\mathbf{r})\mathbf{t}_\mathbf{w}^{(\alpha')}. \tag{29}$$

In order to minimise the residual errors along the boundaries and interfaces, a complete set of basis functions $\Psi_w^{(\alpha')}(\mathbf{r})$ must be used to expand the weighting functions. The choice of basis functions may vary for each boundary but needs to be able to represent any arbitrary field on that boundary. In a conventional WBM domain, all basis functions used to approximate the dynamic field inside domain $\Omega^{(\alpha')}$ are used as weighting functions in the weighted residual equations related to the conditions imposed on $\Gamma^{(\alpha')}$, following the classical Galerkin weighted residual approach. In the case of a multi-level WBM model however, the use of the full basis (with all functions of all levels) is unnecessary since the unbounded basis functions $\Phi_w^{(\alpha,L_i)}$ can accurately approximate any field on the associated truncation circle Γ'_{t,L_i} because they form a complete set for the considered unbounded problem [59]. The same holds for the bounded wave functions $\Phi_w^{(\alpha)}$ along $\partial\Omega^{(\alpha)}$ [41]. The addition of the remaining functions of the other levels would introduce unneeded information to the expansion and could result in a deterioration of the already unfavourable numerical conditioning of the WBM system of equations. Moreover, since this also results in the need to evaluate additional integrals during model construction, the addition of supplementary weighting functions is not only unnecessary but also unwanted. The choice of basis functions which are used to expand the weighting functions in the boundary integral formulation of the multi-level WBM can be summarised as:

$$\Psi_w^{(\alpha')}(\mathbf{r})=\begin{cases}\Phi_w^{(\alpha)}(\mathbf{r}), & \mathbf{r}\in\Gamma^{(\alpha)}\\ \Phi_w^{(\alpha,L_i)}(\mathbf{r}), & \mathbf{r}\in\Gamma'^{(\alpha)}_{t,i}\end{cases}. \tag{30}$$

The theoretical framework presented in this section provides a general concept to efficiently incorporate complex inclusion configurations in a

numerical WBM model which describes the dynamic behaviour of any steady-state dynamic problem which is governed by a (set of) Helmholtz partial differential equation(s). In the two subsequent sections, this general formulation is applied to two specific types of dynamic problems: the interior behaviour of an acoustic cavity and the steady-state elastodynamic behaviour of a perforated membrane. The first class of problems is governed by a single Helmholtz equation, while in the second application it will be shown that the governing system of coupled partial differential equations, the so-called Navier equations [68], can be decomposed in a system of two independent Helmholtz equations, which are mutually coupled through the imposed boundary conditions. For each of these classes of problems, the governing equations and most commonly applied types of boundary conditions are detailed, the selection of a convergent set of wave functions is discussed and the specific underlying multi-level weighted residual formulation is given. Furthermore, for each problem type two verification examples are given and both the accuracy and efficiency of the proposed modelling approach is illustrated with respect to classical Finite and Boundary Element techniques. Even though the general framework from this section includes the possibility to model non-circular inclusions, the discussion in the two following sections is limited to circular inclusion with general boundary conditions in order to enhance the readability of the theoretical derivations in these sections. Moreover, this limitation allows the analysis of the behaviour of the multi-level coupling itself rather than the added modelling complexities related to the use of various types of coupling approaches and continuity conditions to model complex shaped inclusions.

4. Application to two-dimensional interior acoustics

In this section the general multi-level WBM inclusion modelling is applied to the solution of a single Helmholtz equation to study the steady-state dynamic behaviour of an acoustic cavity. The governing equation (and relation between the physical properties of the acoustic fluid and the associated wave number k) and the three most commonly applied types of boundary conditions are discussed. Next, the wave functions used to model this type of problem and the specific multi-level weighted residual formulation are derived. Finally, the multi-level modelling approach is applied to two acoustic problems and the obtained results are compared to classical linear and quadratic element-based numerical modelling techniques to assess the applicability and efficiency of the proposed approach.

4.1. Governing equations and boundary and interface conditions

Consider a general 2D acoustic problem. The acoustic fluid that fills the problem domain is characterised by its density ρ and speed of sound c. The steady-state acoustic pressure $p(\mathbf{r})$ inside the problem domain is governed by the inhomogeneous Helmholtz equation:

$$\nabla^2 p(\mathbf{r}) + k^2 p(\mathbf{r}) = -j\rho\omega\delta(\mathbf{r},\mathbf{r_q})q, \tag{31}$$

with $\omega = 2\pi f$ the circular frequency and $k = \omega/c$ the acoustic wave number. The fluid is excited by a cylindrical acoustic volume velocity source q. The problem boundary Γ is constituted of 2 parts: the finite part of the boundary, Γ_b, and the boundary at infinity, Γ_∞. Based on the three types of commonly applied acoustic boundary conditions, the finite boundary can be further divided in three non-overlapping parts: $\Gamma_b = \Gamma_v \cup \Gamma_p \cup \Gamma_Z$. The following associated boundary condition residuals are defined:

$$\mathbf{r}\in\Gamma_v : R_v(p(\mathbf{r})) = \mathcal{L}_v(p(\mathbf{r})) - \overline{v}_n(\mathbf{r}) = 0, \tag{32}$$

$$\mathbf{r}\in\Gamma_p : R_p(p(\mathbf{r})) = p(\mathbf{r}) - \overline{p}(\mathbf{r}) = 0, \tag{33}$$

$$\mathbf{r}\in\Gamma_Z : R_Z(p(\mathbf{r})) = \mathcal{L}_v(p(\mathbf{r})) - \frac{p(\mathbf{r})}{\overline{Z}_n(\mathbf{r})} = 0, \tag{34}$$

where n is the normal vector pointing out of the acoustic domain and the quantities $\overline{v}_n$, $\overline{p}$ and $\overline{Z}_n$ are, respectively, the imposed normal velocity, pressure and normal impedance values. The velocity operator $\mathcal{L}_v(\bullet)$ is defined as:

$$\mathcal{L}_v(\bullet) = \frac{j}{\rho_0\omega}\frac{\partial \bullet}{\partial n}. \tag{35}$$

At the boundary Γ_∞ the Sommerfeld radiation condition is applied [56], ensuring that no acoustic energy is reflected at infinity and is expressed as:

$$\lim_{|\mathbf{r}|\to\infty}\left(\sqrt{\mathbf{r}}\left(\frac{\partial p(\mathbf{r})}{\partial |\mathbf{r}|} + jkp(\mathbf{r})\right)\right) = 0. \tag{36}$$

Solution of the Helmholtz Eq. (31) together with the associated boundary conditions (32), (33), (34) and (36) yields a unique acoustic pressure field $p(\mathbf{r})$.

To couple the pressure fields in the two acoustic WBM subdomains $\Omega^{(\alpha)}$ and $\Omega^{(\beta)}$ of the partitioned problem domain, Pluymers [69] proposes two types of coupling conditions: direct enforcement of acoustic pressure and velocity continuity and an *equivalent normal velocity* continuity condition. In this paper the latter is applied along $\Gamma_{I,Z}^{(\alpha,\beta)}$ and $\Gamma_{I,Z}^{(\beta,\alpha)}$:

$$R_{I,Z}\left(p^{(\alpha)}(\mathbf{r}), p^{(\beta)}(\mathbf{r})\right) = \mathcal{L}_{eq+}^{(\alpha)}\left(p^{(\alpha)}(\mathbf{r})\right) - \mathcal{L}_{eq-}^{(\beta)}\left(p^{(\beta)}(\mathbf{r})\right) = 0 \quad \mathbf{r}\in\Gamma_{I,Z}^{(\alpha,\beta)}, \tag{37}$$

$$R_{I,Z}\left(p^{(\alpha)}(\mathbf{r}), p^{(\beta)}(\mathbf{r})\right) = \mathcal{L}_{eq+}^{(\beta)}\left(p^{(\beta)}(\mathbf{r})\right) - \mathcal{L}_{eq-}^{(\alpha)}\left(p^{(\alpha)}(\mathbf{r})\right) = 0 \quad \mathbf{r}\in\Gamma_{I,Z}^{(\beta,\alpha)}. \tag{38}$$

The equivalent normal velocity operators $\mathcal{L}_{eq+}^{(\alpha)}(\bullet)$ and $\mathcal{L}_{eq-}^{(\alpha)}(\bullet)$ in this formulation are defined as:

$$\mathcal{L}_{eq+}^{(\alpha)}(\bullet) = \frac{j}{\rho\omega}\frac{\partial \bullet}{\partial n^{(\alpha)}} - \frac{1}{\overline{Z}_{int}}\bullet \tag{39}$$

$$\mathcal{L}_{eq-}^{(\alpha)}(\bullet) = -\frac{j}{\rho\omega}\frac{\partial \bullet}{\partial n^{(\alpha)}} - \frac{1}{\overline{Z}_{int}}\bullet \tag{40}$$

with $\overline{Z}_{int}$ being an impedance coupling factor.

These continuity conditions result in a more stable formulation than using the conventional conditions enforcing pressure and normal velocity continuity, due to the introduction of damping via $\overline{Z}_{int}$ [70]. Pluymers [69] shows that choosing $\overline{Z}_{int}$ to be the characteristic fluid impedance ρc is beneficial for the convergence rate of the method.

4.2. Selection of wave functions

Since the steady-state acoustic pressure inside a cavity is governed by a single Helmholtz equation, the total acoustic pressure field $p^{(\alpha')}(\mathbf{r})$ inside each of the subdomains $\Omega^{(\alpha')}$ can be approximated using the general function expansions for bounded and unbounded problem domains derived in Section 2.3,

$$p^{(\alpha')}(\mathbf{r}) = \mathbf{\Phi}^{(\alpha)}(\mathbf{r})\cdot\mathbf{p}_{\mathbf{w}}^{(\alpha)} + \sum_{L_i=1}^{n_\lambda^{(\alpha)}} \mathbf{\Phi}^{(\alpha,\mathbf{L_i})}(\mathbf{r})\cdot\mathbf{p}_{\mathbf{w}}^{(\alpha,\mathbf{L_i})}. \tag{41}$$

Applying the wave function expansion (12) for the acoustic pressure field $p^{(\alpha)}(\mathbf{r})$ inside all the bounded subdomains $\Omega^{(\alpha)}$ in the

multi-level problem partitioning results in a convergent numerical scheme. For acoustic problems however, the required number of basis functions can be further optimised. Desmet [41] shows that the theoretical convergence of the method is retained even if the functions with a sine as harmonic component are omitted from the expansion. This reduces the number of basis functions by a factor of two if all the functions up to a certain spatial resolution are used and hence results in a substantial increase of the computational efficiency. Based on these observations, the set of wave functions to describe the acoustic pressure field $p^{(\alpha)}(\mathbf{r})$ inside a bounded subdomain $\Omega^{(\alpha)}$ becomes:

$$\Phi_w^{(\alpha)}(\mathbf{r}(x,y)) = \begin{cases} \Phi_{w_r}^{(\alpha)}(x,y) = cos\left(k_{xw_r}^{(\alpha)}x\right)e^{-jk_{yw_r}^{(\alpha)}y} \\ \Phi_{w_s}^{(\alpha)}(x,y) = e^{-jk_{xw_s}^{(\alpha)}x}cos\left(k_{yw_s}^{(\alpha)}y\right) \end{cases}. \tag{42}$$

To model the outgoing wavefields associated to each of the inclusion levels L_i inside subdomain $\Omega^{(\alpha)}$, expansions similar to Eq. (18) are used:

$$\Phi_w^{(\alpha,L_i)}(\mathbf{r}(r,\theta)) = \begin{cases} \Phi_{w_c}^{(\alpha,L_i)}(r,\theta) = H_w^{(2)}(kr)cos(w\theta) \\ \Phi_{w_s}^{(\alpha,L_i)}(r,\theta) = H_w^{(2)}(kr)sin(w\theta) \end{cases}. \tag{43}$$

4.3. Acoustic multi-level weighted residual formulation

The underlying weighted residual formulation for the acoustic multi-level WBM model is constructed using the boundary residuals (32)–(34) and the continuity residuals (37) and (38). Based on a variational analysis of the steady-state acoustic problem, the differential operators $\mathcal{D}_\bullet(^*)$ which need to be applied to the weighting functions $\tilde{p}^{(*)}(\mathbf{r})$ for each of the residuals in the formulation can be identified as either a positive pressure or a negative velocity term:

$$\mathcal{D}_\bullet\left(\tilde{p}^{(*)}(\mathbf{r})\right) = \begin{cases} \tilde{p}^{(*)}(\mathbf{r}) \\ -\mathcal{L}_v^{(*)}(\tilde{p}^{(*)}(\mathbf{r})) \end{cases}. \tag{44}$$

Combining the residuals defined in Section 4.1 with the general multi-level weighted residual formulation derived in Section 3 and these operator definitions results in a variational formulation of the acoustic inclusion problem. The formulation can be written as the sum of three types of contributions:

$$\sum_{\alpha=1}^{N_\Omega}\left[\mathcal{W}_1^{(\alpha)} + \sum_{\beta=1,\beta\neq\alpha}^{N_\Omega}\mathcal{W}_2^{(\alpha,\beta)} + \sum_{L_i}^{n_\lambda^{(\alpha)}}\mathcal{W}_3^{(\alpha,L_i)}\right] = 0. \tag{45}$$

In this formulation, the terms $\mathcal{W}_1^{(\alpha)}$ are related to the boundary conditions applied to the exterior boundary of the bounded subproblem. $\mathcal{W}_2^{(\alpha,\beta)}$ originates from the continuity conditions between the domain $\Omega^{(\alpha')}$ and the adjacent domains. Since both $\mathcal{W}_1^{(\alpha)}$ and $\mathcal{W}_2^{(\alpha,\beta)}$ include conditions which are imposed along the boundary of the bounded submodel (considering only circular scatterers in this derivation), the associated weighting functions are expanded into a set of bounded wave functions $\Phi_w^{(\alpha)}$. The final term $\mathcal{W}_3^{(\alpha,L_i)}$ expresses the boundary conditions which are imposed along the circular boundary of inclusion L_i. The weighting functions in these terms are expanded in a series of unbounded wave functions $\Phi_w^{(\alpha,L_i)}$ associated to the truncation circle of modelling level L_i. In full, these contributions can be written as:

$$\begin{aligned} \mathcal{W}_1^{(\alpha)} &= \int_{\Gamma_v^{(\alpha)}}\tilde{p}^{(\alpha)}R_v\left(p^{(\alpha')}\right)d\Gamma + \int_{\Gamma_Z^{(\alpha)}}\tilde{p}^{(\alpha)}R_Z\left(p^{(\alpha')}\right)d\Gamma + \\ &\quad \int_{\Gamma_p^{(\alpha)}} -\mathcal{L}_v^{(\alpha)}\left(\tilde{p}^{(\alpha)}\right)R_p\left(p^{(\alpha')}\right)d\Gamma \\ \mathcal{W}_2^{(\alpha,\beta)} &= \int_{\Gamma_{IZ}^{(\alpha,\beta)}}\tilde{p}^{(\alpha)}R_{IZ}\left(p^{(\alpha')},p^{(\beta')}\right)d\Gamma \\ \mathcal{W}_3^{(\alpha,L_i)} &= \int_{\Gamma_v^{(\alpha',L_i)}}\tilde{p}^{(\alpha,L_i)}R_v\left(p^{(\alpha')}\right)d\Gamma + \int_{\Gamma_Z^{(\alpha',L_i)}}\tilde{p}^{(\alpha,L_i)}R_Z\left(p^{(\alpha')}\right)d\Gamma + \\ &\quad \int_{\Gamma_p^{(\alpha',L_i)}} -\mathcal{L}_v^{(\alpha')}\left(\tilde{p}^{(\alpha,L_i)}\right)R_p\left(p^{(N_\Omega+\alpha,L_i)}\right)d\Gamma. \end{aligned} \tag{46}$$

Using the weighted residual formulation and the proposed acoustic pressure approximation and weighting function operators and expansions, a linear system of algebraic equations can be constructed which can be solved to obtain the contribution factors of the acoustic wave functions in the numerical approximation of the acoustic pressure field $p(\mathbf{r})$ inside the problem domain.

4.4. Numerical verification example 1: convex acoustic cavity containing a single circular inclusion

This section and the next one discuss two numerical examples which illustrate the applicability of the proposed concept for interior acoustic problems containing one or more circular holes. The results from the WBM calculations are compared to classical element-based numerical modelling approaches based on three types of results:

- Firstly, the single frequency acoustic pressure amplitude distribution inside the entire problem domain is compared to an element-based reference solution.
- Next, an acoustic pressure amplitude response function in a single point inside the cavity is compared to the results of an element-based reference calculation for a frequency range up to 2500 Hz.
- Finally, the efficiency of the proposed modelling framework is assessed by comparing the relative pressure amplitude prediction errors in a single point and the associated computational costs for the WBM and a number of element-based models with a varying mesh density.

In both verification examples the acoustic fluid inside the cavity is air ($c = 340$ m/s, $\rho = 1.225$ kg/m^3). All calculations are performed on a Linux-based 2.66 GHz Intel Xeon system, using the commercial numerical modelling software *LMS/Sysnoise Rev5.6* for the element-based models and a *Matlab R2007b*-based implementation of the multi-level WBM modelling framework.

A first verification example applies the multi-level WBM modelling methodology to a simple problem consisting of a convex acoustic cavity which contains a single circular hole. Fig. 6 shows the problem configuration. The exterior boundaries of the cavity and the hole are considered to be acoustically rigid and the system is excited using an acoustic point source with an amplitude $q = 1$. The cavity is modelled using both the classical linear and quadratic FEM and the newly developed multi-level WBM modelling approach. Several FE models are built for this problem. The FE discretisations consist of a combination of 4- or 8-noded quadrilateral and 3- or 6-noded triangular elements, as is shown in Fig. 7. The details of the models which are used in this verification study are listed in Table 1. For each of the models the number of DOFs, the expected model validity and the computational load needed to calculate a pressure amplitude response function consisting of 2251 frequency lines between 250 Hz and

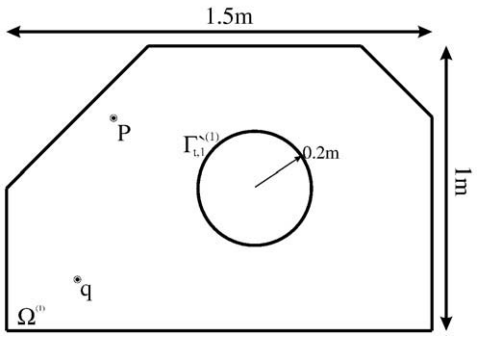

Fig. 6. Acoustic verification 1: convex acoustic cavity with a single inclusion.

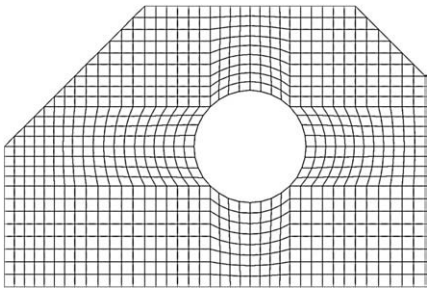

Fig. 7. Acoustic verification 1: FEM discretisation.

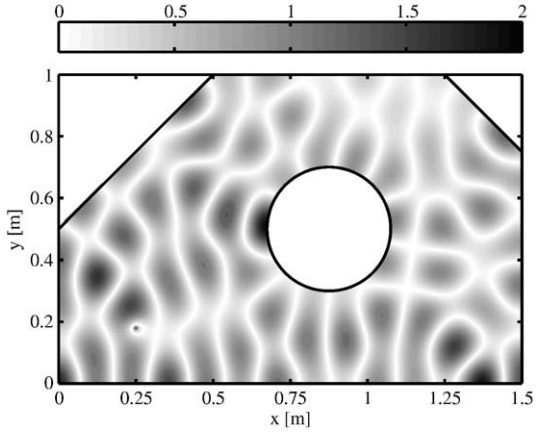

Fig. 8. Acoustic verification 1: pressure amplitude at 1500 Hz [Pa].

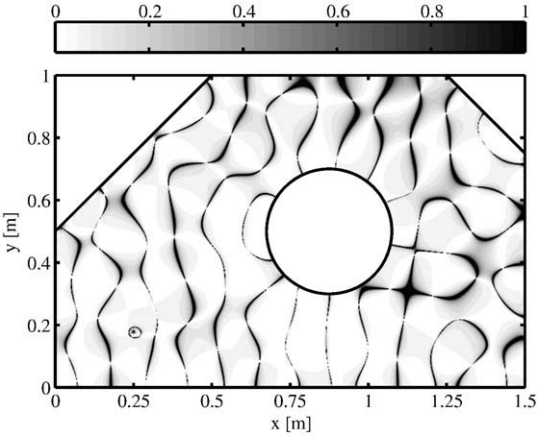

Fig. 9. Acoustic verification 1: pressure amplitude prediction errors at 1500 Hz [%].

2500 Hz is given. The validity of the models is estimated using both a commonly applied rule of thumb, which states that at least 6 linear or 4 quadratic elements are needed to model a single acoustic wavelength, and a more complex rule derived in [2] taking into account numerical pollution effects which become dominant in the mid-frequency range. In the WBM models, the cavity pressure is modelled using a superposition of bounded wave functions (42), and an expansion of unbounded wave functions (43) related to the hole, which are defined by a truncation circle $\Gamma'^{\{1\}}_{t,1}$ which is coinciding with the hole. The total number of functions used in the WBM models is frequency dependent and ranges from 59 at 250 Hz to 557 at 2500 Hz, which corresponds to the application of truncation rule (17) with parameter $T=6$ and is chosen such that the computational load of the model is of the same order of magnitude as that of the most coarse FEM model. The calculation times listed in this table consist of the cost of frequency-dependent operations only, being the time needed to solve the linear system of equations for the FEM and the time to build and solve the multi-level system matrices for the WBM. The time to calculate the FEM system matrices is not taken into account since this is a one-time operation whose computational load is negligible when the model is solved at many frequencies.

The contours in Fig. 8 show the acoustic pressure amplitude inside the cavity at 1500 Hz, computed using the multi-level WBM. In Fig. 9, the relative error ε_{rel}, as defined in Eq. (47) of this pressure amplitude with respect to the results of the most detailed quadratic FEM model is shown.

$$\varepsilon_{rel} = \frac{||p^{(\alpha')}(\mathbf{r})| - |p_{ref}(\mathbf{r})||}{|p_{ref}(\mathbf{r})|} \tag{47}$$

with $|p_{ref}(\mathbf{r})|$ the acoustic pressure amplitude reference. The acoustic amplitude prediction errors remain well within the range of 0–1%, except at the pressure nodal lines, where the error calculation itself is inaccurate due to almost-zero division.

Fig. 10 compares the frequency response function in the frequency range between 250 and 2500 Hz of the acoustic pressure amplitude in the response point P (0.375 m, 0.75 m) indicated in Fig. 6 for the quadratic FEM reference model and the WBM model. The good agreement between the WBM results and the FEM reference is evident from this figure.

A more detailed comparison is made in Fig. 11 where the frequency-dependent pressure amplitude errors in the response

Table 1
Model information for acoustic verification example 1.

	Element order	Element size [mm]	#DOFs (=#nodes)	Mesh validity		Calculation time [s]
				Fixed # el./λ [Hz]	[2] [Hz]	
FEM	Linear	10	13,302	5,422	1,018	720
	Quadratic	15	16,592	7,215	2,500	1,327
	Quadratic	6	106,823	18,038	5,205	42,750
	Quadratic	4	235,783	27,056	7,198	/
WBM	/	/	59–557	/	/	664

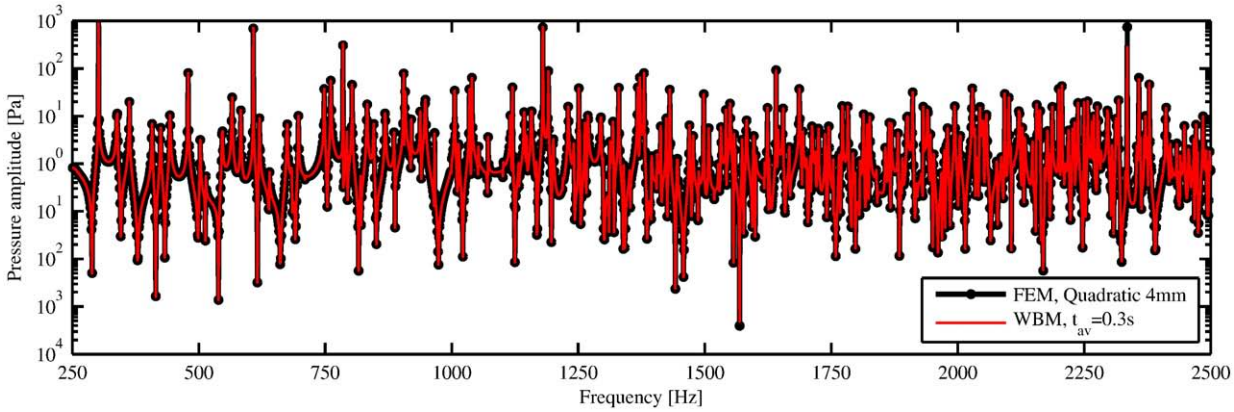

Fig. 10. Acoustic verification 1: pressure amplitude [Pa] comparison: WBM model and FEM reference.

point *P* for the three FEM models and the WBM model are shown. As shown in the bottom figure, the WBM model is valid over the entire frequency range presented here. The spikes in the error spectrum at certain frequencies originate from the fact that the acoustic pressure amplitude at resonance is undetermined due to the lack of damping in the system. It is clear that the WBM result (bottom figure) is far more accurate than the one obtained by the linear FEM model with the same calculation time (top figure). The second figure illustrates the advantage of using a higher-order FEM model. In this figure the prediction errors for a quadratic FEM model with a comparable computational load to that of the linear FEM model is given. The quadratic model is valid up to approximately 1250 Hz while the linear model is only able to accurately predict the acoustic behaviour up to 500 Hz. As shown in the third figure from the top, the quadratic FEM mesh needs to be refined in order to obtain the same overall average prediction accuracy as the WBM calculation. This results in an average computation time of 19 s per frequency, while the WBM model only needs 0.3 s per frequency to obtain a similar overall prediction accuracy. It can be concluded that for this verification example the newly developed multi-level WBM modelling concept is about 60 times quicker than the quadratic FEM. This clearly illustrates the advantageous properties of the proposed modelling concept.

4.5. Numerical verification example 2: non-convex acoustic cavity containing multiple circular inclusions

In a second verification example, the multi-level modelling concept is applied to the bounded acoustic problem shown in Fig. 12. A concave cavity which contains seven circular holes is excited using a constant acoustic normal velocity distribution along the left edge. One of the holes inside the cavity is covered with an acoustic absorbing material, which is modelled by applying an acoustic normal impedance boundary condition (34) along the edge of the hole. A normal impedance value $\overline{Z} = 441 - 1241j\frac{Pas}{m}$ is imposed. The concave shape of the cavity requires the WBM model to consist of two bounded subdomains: one bounded WBM subdomain is used to model the rectangular domain to the left and one bounded subdomain, which constitutes the bounded level of a multi-level domain, describes the acoustic behaviour of the convex cavity to the right. Both submodels are linked to each other using the

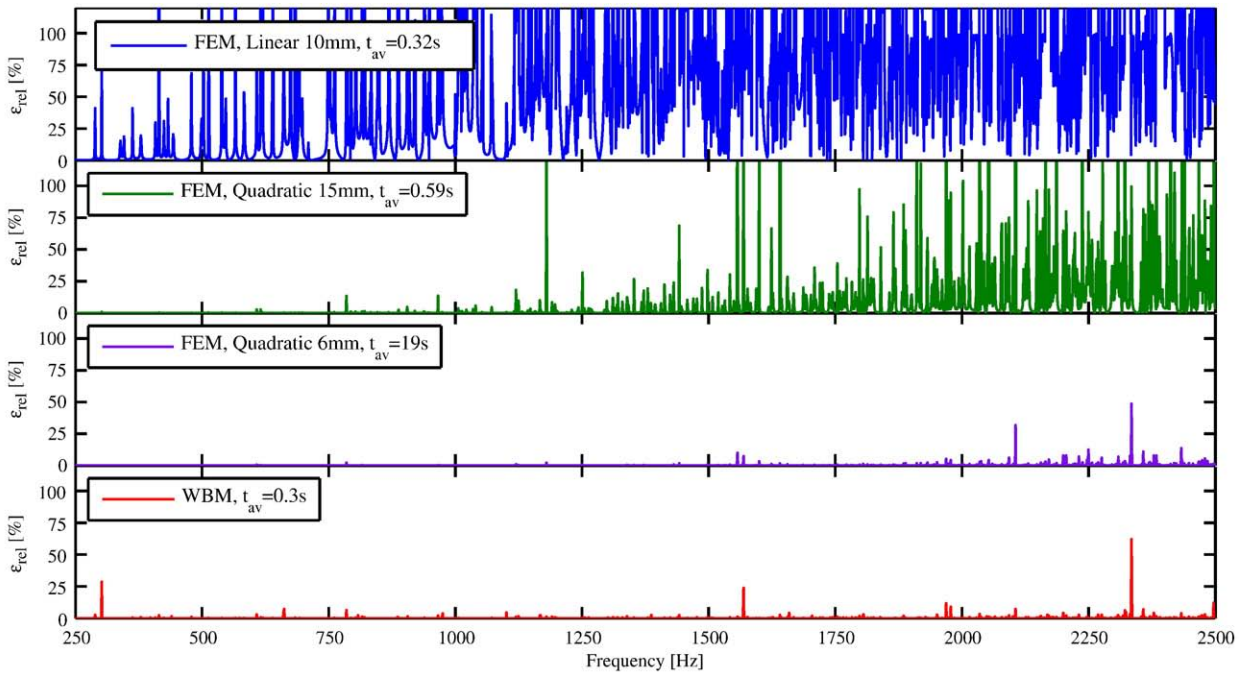

Fig. 11. Acoustic verification 1: pressure amplitude error function [%] comparison: WBM and FEM models.

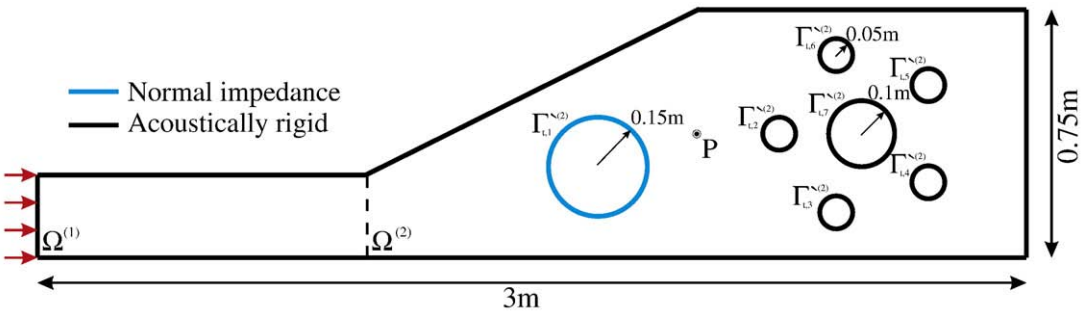

Fig. 12. Acoustic verification 2: concave acoustic cavity containing multiple circular inclusions.

Table 2
Model information for acoustic verification example 2.

	Element Size [mm]	#DOFs (=#nodes)	Mesh validity: 6 el./λ [Hz]	Mesh validity: [2] [Hz]	Calculation time [s]
BEM	7.5	1,367	7,215	979	4,600
	2.5	4,105	21,645	2,037	47,200
	1	10,258	54,113	3,752	/
WBM	/	143–675	/	/	2,340

continuity conditions (37) and (38). The second subdomain contains seven holes, all of which are introduced in the WBM model by assigning a separate unbounded level to them. Similar to the first example, unbounded wave function sets based on truncation circles which coincide with the holes are used in the multi-level model. Since the complex geometry of the problem may result in large mesh distortions when the FEM is used to model this problem, the linear BEM is used to obtain a reference solution and to compare the multi-level modelling concept to classical element-based methodologies. The model details for the various BEM models are given in Table 2, the 1 mm model is used as a reference. This table also lists the details of the WBM model with truncation parameter $T=4$, which is again created such that the total calculation time for an acoustic pressure response function consisting of 2001 frequency lines between 500 Hz and 2500 Hz is the same order of magnitude as the computational load of the most coarse BEM model. Since the BEM system matrices are frequency dependent, the BEM calculation times comprise the times needed to build and to solve the system matrices.

The contours in Fig. 13 show the amplitude of the acoustic pressure inside the cavity at 1500 Hz, calculated using the WBM. In Fig. 14, the

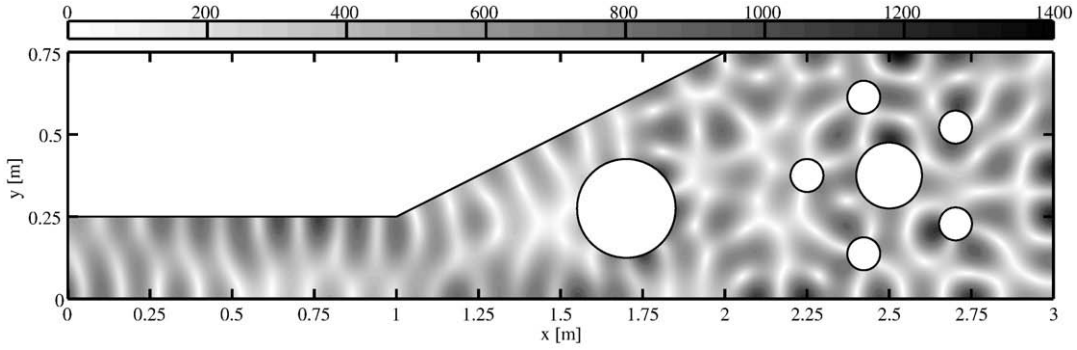

Fig. 13. Acoustic verification 2: pressure amplitude at 1500 Hz [Pa].

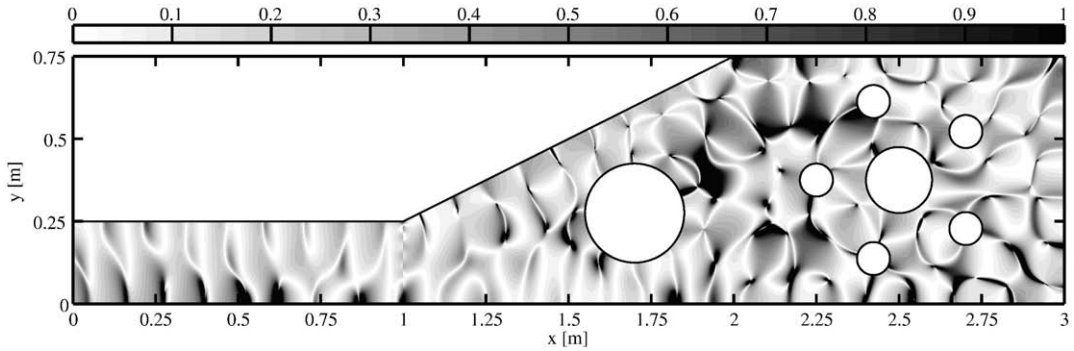

Fig. 14. Acoustic verification 2: pressure amplitude prediction errors at 1500 Hz [%].

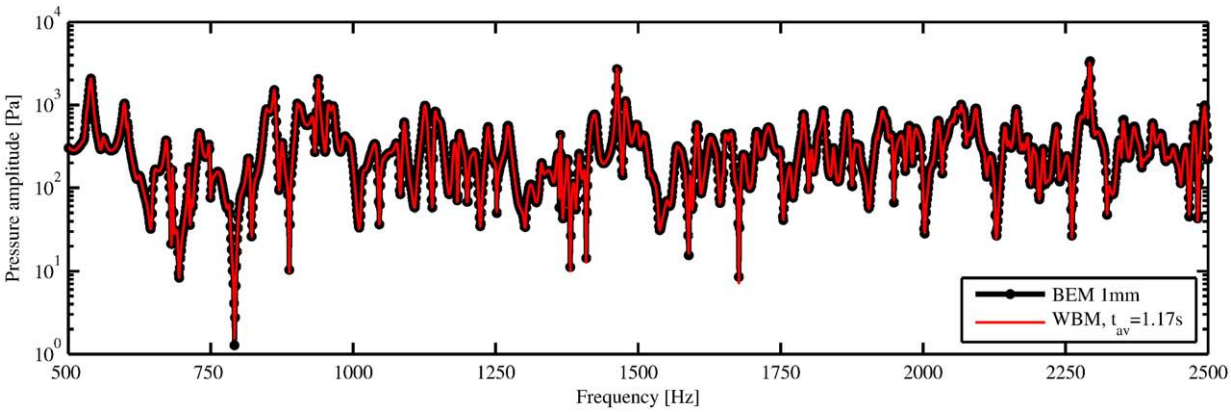

Fig. 15. Acoustic verification 2: pressure amplitude [Pa] comparison: WBM model and FEM reference.

relative prediction error of this pressure result is again compared to the BEM reference. The acoustic amplitude prediction errors remain well within the range of 0–1%. Like in the first verification study, higher errors are observed at the pressure nodal lines, where the error calculation is inaccurate.

Fig. 15 compares the acoustic pressure amplitude in the frequency range between 500 Hz and 2500 Hz in the response point P (2 m, 0.375 m) indicated in Fig. 12 for the BEM reference model and the WBM model. The figure shows a good agreement between the WBM results and the BEM reference.

A more detailed study of the accuracy and performance of the multi-level WBM modelling framework presented in Fig. 16 shows very similar behaviour as observed for the first verification example. Also for this more complex problem the WBM prediction result (bottom figure) is far more accurate than the one obtained by the linear BEM model with the same calculation time (top figure). As shown in the middle figure, refining the BEM model results in a better overall average prediction accuracy. This results in an average computation time of 19 s per frequency, while the WBM model only needs 1.17 s per frequency to obtain a similar overall prediction accuracy at low frequencies and a much better accuracy at the upper end of the frequency range. It can be concluded that for this verification example the newly developed multi-level WBM modelling concept requires about 20 times less computational effort to attain the same prediction accuracy as the linear BEM. This illustrates that the proposed modelling concept retains its advantageous properties when it is applied to the study of more complex systems.

5. Application to two-dimensional elastodynamics of perforated solids

In this section the general multi-level WBM inclusion modelling concept is applied to the solution of the steady-state dynamic deformations of a perforated membrane. Firstly, the governing system of two coupled partial differential equations is decomposed into two uncoupled Helmholtz equations by means of a transformation of the primary variables and the three types of boundary conditions which link the fields described by both equations together are discussed. Next, the wave functions used to model the behaviour of both Helmholtz fields and the specific multi-level weighted residual formulation are derived. Finally, the multi-level modelling approach is applied to two dynamic perforated membrane problems and the obtained results are compared to classicallinear and quadratic element-based numerical modelling techniques to assess the applicability and efficiency of the proposed approach.

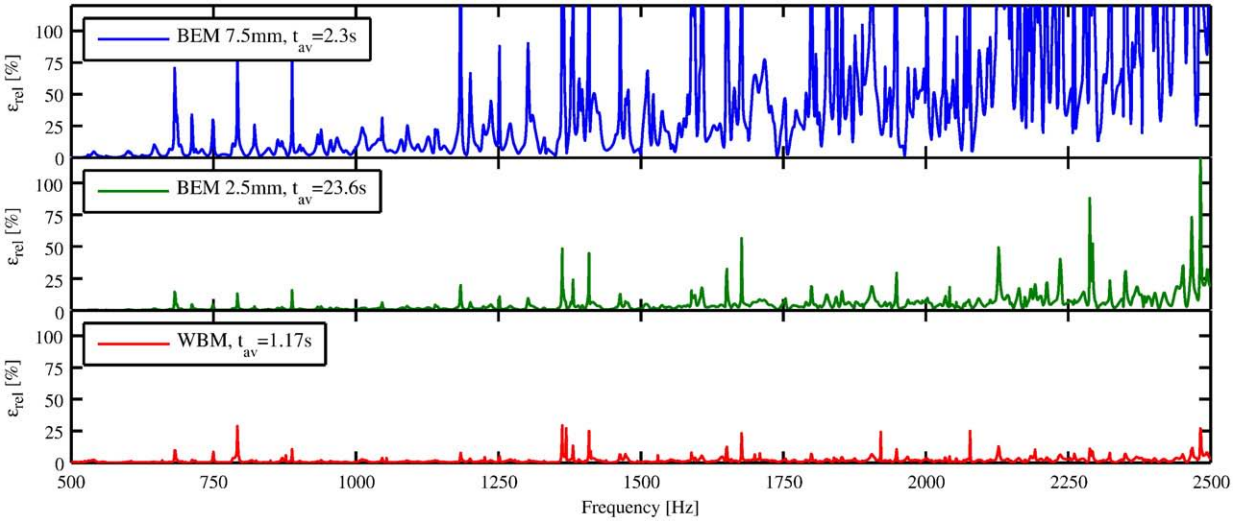

Fig. 16. Acoustic verification 2: pressure amplitude error function [%] comparison: WBM and FEM models.

5.1. Governing equations and boundary and interface conditions

Consider a general interior structural dynamic membrane problem. The Navier system of coupled partial differential equations describes the dynamic in-plane displacements in a two-dimensional solid [68]:

$$\begin{cases} \dfrac{\partial^2 w_x}{\partial x^2} + \dfrac{1-\nu}{2}\dfrac{\partial^2 w_x}{\partial y^2} + \dfrac{1+\nu}{2}\dfrac{\partial^2 w_y}{\partial x \partial y} + \dfrac{\rho(1-\nu^2)\omega^2}{E(1+j\eta)} w_x = 0, \\ \dfrac{\partial^2 w_y}{\partial y^2} + \dfrac{1-\nu}{2}\dfrac{\partial^2 w_y}{\partial x^2} + \dfrac{1+\nu}{2}\dfrac{\partial^2 w_x}{\partial x \partial y} + \dfrac{\rho(1-\nu^2)\omega^2}{E(1+j\eta)} w_y = 0, \end{cases} \tag{48}$$

with E the Young's modulus, ν the Poisson-coefficient, ρ the density, η the damping ratio and ω the circular frequency.

Many modern numerical simulation approaches, like the FEM, directly discretise this system of partial differential equations to derive the structural model matrices. The WBM, on the other hand, applies an expansion in terms of exact analytical solutions of the governing equations as basis functions. In order to enable the derivation of such a set of solutions of the coupled equations (48), Vanmaele [65] proposes to decompose the total structural dynamic strain field $\mathbf{S}$ into a dilatational and a rotational component e and Ω, from which the two displacement components can be derived by means of the following differential relationship:

$$\mathbf{w}(\mathbf{r}) = \begin{Bmatrix} w_x \\ w_y \end{Bmatrix} = -\frac{1}{k_l^2}\nabla e + \frac{1}{k_t^2}\nabla \times \Omega, \tag{49}$$

with ∇ the gradient operator, $\nabla\times$ the curl operator. This decomposition converts the coupled system of Navier Eq. (48) into two uncoupled Helmholtz-type equations,

$$\nabla^2 e + k_l^2 e = 0, \tag{50}$$

$$\nabla^2 \Omega + k_t^2 \Omega = 0, \tag{51}$$

with the in-plane longitudinal and shear wave numbers k_l and k_t defined as,

$$k_l = \omega\sqrt{\frac{\rho(1-\nu^2)}{E(1+j\eta)}} \quad \text{and} \quad k_t = \omega\sqrt{\frac{2\rho(1+\nu)}{E(1+j\eta)}}. \tag{52}$$

The differential operators, needed to reconstruct the in-plane normal and tangential displacement, and the in-plane normal and tangential force from the strain field $\mathbf{S}$ are defined as follows,

$$\mathcal{L}_{w_n} = \left[-\frac{1}{k_l^2}\frac{\partial}{\partial n} \quad \frac{1}{k_t^2}\frac{\partial}{\partial s} \right], \tag{53}$$

$$\mathcal{L}_{w_s} = \left[-\frac{1}{k_l^2}\frac{\partial}{\partial s} \quad -\frac{1}{k_t^2}\frac{\partial}{\partial n} \right], \tag{54}$$

$$\mathcal{L}_{T_n} = \left[-\frac{1}{k_l^2}\frac{Eh(1+j\eta)}{1-\nu^2}\left(\frac{\partial^2}{\partial n^2} + \nu\frac{\partial^2}{\partial s^2}\right) \quad \frac{1}{k_t^2}\frac{Eh(1+j\eta)}{1+\nu}\frac{\partial^2}{\partial n \partial s} \right], \tag{55}$$

$$\mathcal{L}_{T_s} = \left[-\frac{1}{k_l^2}\frac{Eh(1+j\eta)}{1+\nu}\frac{\partial^2}{\partial n \partial s} \quad \frac{1}{k_t^2}\frac{Eh(1+j\eta)}{2(1+\nu)}\left(\frac{\partial^2}{\partial s^2} - \frac{\partial^2}{\partial n^2}\right) \right], \tag{56}$$

where n and s are the in-plane normal and in-plane tangential directions of the plate boundary Γ.

By applying the decomposition proposed above, the mutual coupling between the two strain field components is entirely contained within the boundary and continuity conditions which are specified along the subdomain boundaries. The most commonly applied types of boundary conditions for the dynamic in-plane displacements of a 2D solid include a combination of the normal and tangential components of the dynamic deformations and/or forces along the domain boundaries. The corresponding error residuals are defined as

$$\begin{aligned} R_{w_n} &= \mathcal{L}_{w_n}\begin{bmatrix} e \\ \Omega \end{bmatrix} - \overline{w}_n \\ R_{w_s} &= \mathcal{L}_{w_s}\begin{bmatrix} e \\ \Omega \end{bmatrix} - \overline{w}_s \\ R_{T_n} &= \mathcal{L}_{T_n}\begin{bmatrix} e \\ \Omega \end{bmatrix} - \overline{T}_n \\ R_{T_s} &= \mathcal{L}_{T_s}\begin{bmatrix} e \\ \Omega \end{bmatrix} - \overline{T}_s \end{aligned} \tag{57}$$

with $\overline{w}_n$, $\overline{w}_s$, $\overline{T}_n$ and $\overline{T}_s$ the prescribed normal and shear displacements and forces.

Since the membrane equations consist of two second-order partial differential equations, two of the above types of boundary conditions must be specified at each point of the plate boundary Γ in order to obtain a well-posed problem. Based on three commonly used combinations of conditions, the entire bounded boundary of the solid can be divided into three non-overlapping parts: $\Gamma_b = \Gamma_f \cup \Gamma_w \cup \Gamma_{sym}$.

- Along the *force* boundary Γ_f, both force residuals R_{T_n} and R_{T_s} are set to be zero.
- Along the *displacement* boundary Γ_w, both displacement residuals R_{w_n} and R_{w_s} are set to be zero.
- Along a *symmetry* boundary Γ_{sym}, The normal displacement and the shear force are forced to zero, using the residuals R_{w_n} and R_{T_s} with prescribed values $\overline{w}_n = 0$ and $\overline{T}_s = 0$.

At the boundary Γ_∞ at infinity the well-known Kupradze radiation condition is applied [71], ensuring that no structural energy is reflected at infinity and is expressed as

$$\lim_{|\mathbf{r}|\to\infty}\left(\sqrt{\mathbf{r}}\left(\frac{\partial \mathbf{u}^{\mathbf{P}}(\mathbf{r})}{\partial |\mathbf{r}|} + jk_l \mathbf{u}^{\mathbf{P}}(\mathbf{r})\right)\right) = 0 \tag{58}$$

$$\lim_{|\mathbf{r}|\to\infty}\left(\sqrt{\mathbf{r}}\left(\frac{\partial \mathbf{u}^{\mathbf{S}}(\mathbf{r})}{\partial |\mathbf{r}|} + jk_t \mathbf{u}^{\mathbf{S}}(\mathbf{r})\right)\right) = 0 \tag{59}$$

with $\mathbf{u}^{\mathbf{P}}(\mathbf{r}) = -k_l^{-2}\nabla(\nabla \cdot \mathbf{u}(\mathbf{r}))$ the longitudinal and $\mathbf{u}^{\mathbf{S}}(\mathbf{r}) = k_t^{-2}\nabla\times(\nabla\times\mathbf{u}(\mathbf{r}))$ the rotational part of the dynamic response field, which correspond to radiated *P*- and *S*-waves respectively [72].

Solution of the system of Helmholtz Eqs. (50)–(51) together with the associated boundary and radiation conditions yields a unique dynamic deformation field $\mathbf{w}(\mathbf{r})$.

Partitioning of the elastodynamic problem using the WBM approach results in the creation of a number of domain interfaces along which the dynamic deformations in adjacent subdomains $\Omega^{(\alpha)}$ and $\Omega^{(\beta)}$ need to be matched. In the WBM approach for elastodynamics, this coupling is most commonly achieved by imposing the continuity of both displacement components on one of the subdomains, while the force equilibrium is enforced on the other subdomain:

$$R_{I,w}\left(\mathbf{u}^{(\alpha)}(\mathbf{r}), \mathbf{u}^{(\beta)}(\mathbf{r})\right) = \begin{cases} \mathcal{L}_{w_n}^{(\alpha)}\mathbf{S}^{(\alpha)}(\mathbf{r}) - \mathcal{L}_{w_n}^{(\beta)}\mathbf{S}^{(\beta)}(\mathbf{r}) = 0 \\ \mathcal{L}_{w_s}^{(\alpha)}\mathbf{S}^{(\alpha)}(\mathbf{r}) - \mathcal{L}_{w_s}^{(\beta)}\mathbf{S}^{(\beta)}(\mathbf{r}) = 0 \end{cases} \quad \mathbf{r}\in\Gamma_{I,w}^{(\alpha,\beta)}, \tag{60}$$

$$R_{I,T}\left(\mathbf{u}^{(\beta)}(\mathbf{r}),\mathbf{u}^{(\alpha)}(\mathbf{r})\right)=\begin{cases}\mathcal{L}_{T_n}^{(\beta)}\mathbf{S}^{(\beta)}(\mathbf{r})-\mathcal{L}_{T_n}^{(\alpha)}\mathbf{S}^{(\alpha)}(\mathbf{r})=0\\ \mathcal{L}_{T_s}^{(\beta)}\mathbf{S}^{(\beta)}(\mathbf{r})-\mathcal{L}_{T_s}^{(\alpha)}\mathbf{S}^{(\alpha)}(\mathbf{r})=0\end{cases}\quad \mathbf{r}\in\Gamma_{I,T}^{(\beta,\alpha)}. \tag{61}$$

5.2. Selection of wave functions

Since each of the steady-state structural strain components inside the problem domain is governed by an independent Helmholtz equation, the total strain field $\mathbf{S}^{(\alpha')}(\mathbf{r})$ inside each of the subdomains $\Omega^{(\alpha')}$ can be approximated using two independent general function expansions for bounded and unbounded problem domains like the ones derived in Section 2.3.

$$\mathbf{S}^{(\alpha')}(\mathbf{r})=\begin{bmatrix}e\\ \Omega\end{bmatrix}=\begin{bmatrix}\boldsymbol{\Phi}_{\mathbf{l}}^{(\alpha)}(\mathbf{r})\cdot\mathbf{u}_{\mathbf{l}}^{(\alpha)}+\sum_{L_i=1}^{n_\lambda^{(\alpha)}}\boldsymbol{\Phi}_{\mathbf{l}}^{(\alpha,\mathbf{L_i})}(\mathbf{r})\cdot\mathbf{u}_{\mathbf{l}}^{(\alpha,\mathbf{L_i})}\\ \boldsymbol{\Phi}_{\mathbf{t}}^{(\alpha)}(\mathbf{r})\cdot\mathbf{u}_{\mathbf{t}}^{(\alpha)}+\sum_{L_i=1}^{n_\lambda^{(\alpha)}}\boldsymbol{\Phi}_{\mathbf{t}}^{(\alpha,\mathbf{L_i})}(\mathbf{r})\cdot\mathbf{u}_{\mathbf{t}}^{(\alpha,\mathbf{L_i})}\end{bmatrix}. \tag{62}$$

Based on this expansion, the elastodynamic displacement fields $\mathbf{w}^{(\alpha)}$ can be easily obtained by applying the corresponding differential operators to the proposed strain expansions.

Applying the wave function expansion (12) for the elastodynamic strain fields $\mathbf{S}^{(\alpha)}(\mathbf{r})$ inside all the bounded subdomains $\Omega^{(\alpha)}$ in the multi-level problem partitioning results in a convergent numerical scheme. The optimisation of the number of wave functions for the strain fields in the bounded domains by omitting the sine-type harmonic components also retains the theoretical convergence of the WBM modelling approach. Vanmaele [65] shows however that in practical applications the obtained convergence rate of the method is significantly higher when using the full set of basis functions. Consequently, the full set of bounded wave functions is used to expand the bounded strain fields $\mathbf{S}^{(\alpha)}$:

$$\Phi_{\{l,t\}}^{(\alpha)}(\mathbf{r}(x,y))=\begin{cases}\Phi_{\{l,t\}_r}^{(\alpha)}(x,y)=\left\{sin\left(k_{x\{l,t\}_r}^{(\alpha)}x\right),cos\left(k_{x\{l,t\}_r}^{(\alpha)}x\right)\right\}e^{-jk_{y\{l,t\}_r}^{(\alpha)}y}\\ \Phi_{\{l,t\}_s}^{(\alpha)}(x,y)=e^{-jk_{x\{l,t\}_s}^{(\alpha)}x}\left\{sin\left(k_{x\{l,t\}_r}^{(\alpha)}x\right),cos\left(k_{y\{l,t\}_s}^{(\alpha)}y\right)\right\}\end{cases}. \tag{63}$$

To describe the outgoing strain fields associated to each of the inclusion levels L_i inside subdomain $\Omega^{(\alpha)}$, expansions similar to Eq. (18), which result in displacement fields which a priory fulfill the Kupradze non-reflection boundary conditions along Γ_∞ are used:

$$\Phi_{\{l,t\}}^{(\alpha,L_i)}(\mathbf{r}(r,\theta))=\begin{cases}\Phi_{\{l,t\}_c}^{(\alpha,L_i)}(r,\theta)=H_{\{l,t\}}^{(2)}\left(k_{\{l,t\}}r\right)cos(\{l,t\}\theta)\\ \Phi_{\{l,t\}_s}^{(\alpha,L_i)}(r,\theta)=H_{\{l,t\}}^{(2)}\left(k_{\{l,t\}}r\right)sin(\{l,t\}\theta)\end{cases}. \tag{64}$$

5.3. Membrane multi-level weighted residual formulation

The underlying weighted residual formulation for the elastodynamic multi-level WBM model is constructed based on the boundary residuals (57) and the continuity residuals (60) and (61). Based on a variational analysis of the steady-state elastodynamic problem, the differential operators which need to be applied to the weighting functions $\tilde{\mathbf{S}}^{(\bullet)}(\mathbf{r})$ for each of the residuals in the formulation can be identified as either a positive displacement or a negative force term:

$$\mathcal{D}_\bullet\left(\tilde{\mathbf{S}}^{(*)}(\mathbf{r})\right)=\begin{cases}\mathcal{L}_{w_n}\tilde{\mathbf{S}}^{(*)}(\mathbf{r})\\ \mathcal{L}_{w_s}\tilde{\mathbf{S}}^{(*)}(\mathbf{r})\\ -\mathcal{L}_{T_n}\tilde{\mathbf{S}}^{(*)}(\mathbf{r})\\ -\mathcal{L}_{T_s}\tilde{\mathbf{S}}^{(*)}(\mathbf{r})\end{cases}. \tag{65}$$

Combining the defined residuals in Section 5.1 with the general multi-level weighted residual formulation derived in Section 3 and the results from the variational analysis, yields a variational formulation of the elastodynamic inclusion problem. This formulation can again be written as the sum of three types of contributions:

$$\sum_{\alpha=1}^{N_\Omega}\left[\mathcal{W}_1^{(\alpha)}+\sum_{\beta=1,\beta\neq\alpha}^{N_\Omega}\mathcal{W}_2^{(\alpha,\beta)}+\sum_{L_i}^{n_\lambda^{(\alpha)}}\mathcal{W}_3^{(\alpha,L_i)}\right]=0. \tag{66}$$

In this formulation, the terms $\mathcal{W}_1^{(\alpha)}$ are related to the boundary conditions applied to the exterior boundary of the bounded subproblem. $\mathcal{W}_2^{(\alpha,\beta)}$ originates from the continuity conditions between the domain $\Omega^{(\alpha')}$ and the adjacent domains. Since both $\mathcal{W}_1^{(\alpha)}$ and $\mathcal{W}_2^{(\alpha,\beta)}$ include conditions which are imposed along the boundary of the bounded submodel (considering only circular scatterers in this derivation), the associated weighting functions are expanded into a set of bounded wave functions $\Phi_{\{l,t\}}^{(\alpha)}$. The final term $\mathcal{W}_3^{(\alpha,L_i)}$ expresses the boundary conditions which are imposed along the circular boundary of inclusion L_i. The weighting functions in these terms are expanded in a series of unbounded wave functions $\Phi_{\{l,t\}}^{(\alpha,L_i)}$ associated to the truncation circle of modelling level L_i. In full, these contributions can be written as:

$$\begin{aligned}\mathcal{W}_1^{(\alpha)}=&\int_{\Gamma_f^{(\alpha)}}\mathcal{L}_{w_n}\left(\tilde{\mathbf{S}}^{(\alpha)}\right)R_{T_n}\left(\mathbf{S}^{(\alpha')}\right)d\Gamma+\int_{\Gamma_f^{(\alpha)}\cup\Gamma_{sym}^{(\alpha)}}\mathcal{L}_{w_s}\left(\tilde{\mathbf{S}}^{(\alpha)}\right)R_{T_s}\left(\mathbf{S}^{(\alpha')}\right)d\Gamma\\&+\int_{\Gamma_w^{(\alpha)}}-\mathcal{L}_{T_n}\left(\tilde{\mathbf{S}}^{(\alpha)}\right)R_{w_n}\left(\mathbf{S}^{(\alpha')}\right)d\Gamma\\&+\int_{\Gamma_w^{(\alpha)}\cup\Gamma_{sym}^{(\alpha)}}-\mathcal{L}_{T_s}\left(\tilde{\mathbf{S}}^{(\alpha)}\right)R_{w_s}\left(\mathbf{S}^{(\alpha')}\right)d\Gamma\end{aligned}$$

$$\begin{aligned}\mathcal{W}_2^{(\alpha,\beta)}=&\int_{\Gamma_{I,T}^{(\alpha,\beta)}}\mathcal{L}_{w_n}\left(\tilde{\mathbf{S}}^{(\alpha)}\right)R_{I,T_n}\left(\mathbf{S}^{(\alpha')},\mathbf{S}^{(\beta')}\right)d\Gamma\\&+\int_{\Gamma_{I,T}^{(\alpha,\beta)}}\mathcal{L}_{w_s}\left(\tilde{\mathbf{S}}^{(\alpha)}\right)R_{I,T_s}\left(\mathbf{S}^{(\alpha')},\mathbf{S}^{(\beta')}\right)d\Gamma\\&+\int_{\Gamma_{I,w}^{(\alpha,\beta)}}-\mathcal{L}_{T_n}\left(\tilde{\mathbf{S}}^{(\alpha)}\right)R_{I,w_n}\left(\mathbf{S}^{(\alpha')},\mathbf{S}^{(\beta')}\right)d\Gamma\\&+\int_{\Gamma_{I,w}^{(\alpha,\beta)}}-\mathcal{L}_{T_s}\left(\tilde{\mathbf{S}}^{(\alpha)}\right)R_{I,w_s}\left(\mathbf{S}^{(\alpha')},\mathbf{S}^{(\beta')}\right)d\Gamma\end{aligned}$$

$$\begin{aligned}\mathcal{W}_3^{(\alpha,L_i)}=&\int_{\Gamma_f^{(\alpha',L_i)}}\mathcal{L}_{w_n}\left(\tilde{\mathbf{S}}^{(\alpha,L_i)}\right)R_{T_n}\left(\mathbf{S}^{(\alpha')}\right)d\Gamma\\&+\int_{\Gamma_f^{(\alpha',L_i)}}\mathcal{L}_{w_s}\left(\tilde{\mathbf{S}}^{(\alpha,L_i)}\right)R_{T_s}\left(\mathbf{S}^{(\alpha')}\right)d\Gamma\\&+\int_{\Gamma_w^{(\alpha',L_i)}}-\mathcal{L}_{T_n}\left(\tilde{\mathbf{S}}^{(\alpha,L_i)}\right)R_{w_n}\left(\mathbf{S}^{(\alpha')}\right)d\Gamma+\int_{\Gamma_w^{(\alpha',L_i)}}\\&-\mathcal{L}_{T_s}\left(\tilde{\mathbf{S}}^{(\alpha,L_i)}\right)R_{w_s}\left(\mathbf{S}^{(\alpha')}\right)d\Gamma.\end{aligned} \tag{67}$$

Using the weighted residual formulation and the proposed elastodynamic strain approximations and weighting function operators and expansions, a linear system of algebraic equations can be constructed which can be solved to obtain the contribution factors of the structural wave functions to the numerical approximation of the elastodynamic deformation field $\mathbf{u}(\mathbf{r})$ inside the problem domain.

5.4. Numerical verification example 1: square membrane containing a single circular hole

The potential of the WBM extended with the multi-level concept is demonstrated by means of two numerical verification examples. Consider the square plate with circular hole shown in Fig. 17. Using the multi-level approach for elastodynamic problems presented above, it is possible to use only one bounded domain and one unbounded modelling level to accurately model this problem.

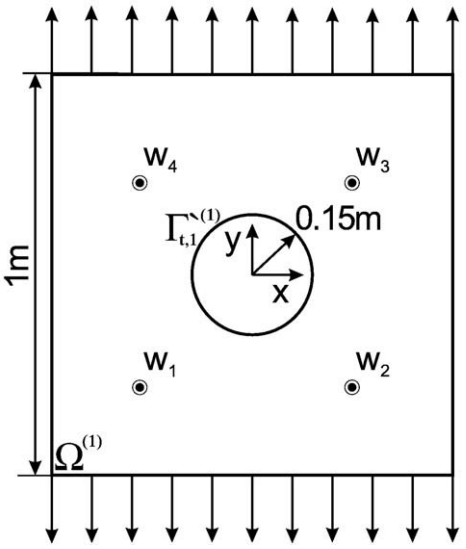

Fig. 17. Elastodynamic verification 1: square plate with circular hole.

The plate is loaded by a unit line load at the top and bottom of the plate and has a thickness of 0.001 m. The material is an aluminium alloy ($E=70\cdot 109$ N/m^2, $\nu=0.3$, $\rho=2{,}790$ kg/m^3). The following response points are considered: $w_1(-0.25\text{ m}, -0.25\text{ m})$, $w_2(0.25\text{ m}, -0.25\text{ m})$, $w_3(0.25\text{ m}, 0.25\text{ m})$ and $w_4(-0.25\text{ m}, 0.25\text{ m})$, as indicated in Fig. 17.

The plate is modelled using both linear and quadratic FE and a number of multi-level WB models. The WB models do not require a rediscretisation in order to refine the model. The perforated membrane can be modelled by constructing a multi-level WB model which combines a single square bounded subdomain and 1 unbounded level with a truncation circle which coincides with the geometry of the hole. Variation of the truncation parameter T in Eq. (17) can again be used to create several WB models with different numbers of structural WB degrees of freedom for the bounded subdomain. The number of unbounded functions in the second model level is chosen such that the spatial resolution of the bounded and unbounded wave functions are approximately the same.

In order to study the convergence behaviour of the FEM, the entire perforated membrane is modelled using both linear and quadratic FEM models. The linear models use 4-noded quadrilateral elements to discretise the problem domain, while the quadratic FE models are built using 8-noded quadrilateral membrane elements. A baseline model with an average discretisation dimension $h\approx 0.025$ m is continuously refined in order to generate all the models, the details of which are given in Table 3. The most detailed quadratic FE model (model number 13) serves as a reference solution when comparing the computational accuracy of the different models at a single frequency. When looking at the displacement prediction results for a large number of frequencies in a frequency response analysis, the computational effort for the use of this reference becomes prohibitively large and the quadratic FE model number 9 is used as a reference solution. In Table 3 h_{max} is the length of the longest side of a finite element in the discretisation, and t_{solve} is the frequency-independent CPU time needed to solve the different models for a single frequency. The commercial FEM software *MD.Nastran R3b* is used to carry out the FEM analyses and all calculations are performed on a 2.66 GHz Intel Xeon based Linux-system with 32 gigabytes of RAM.

To illustrate that the multi-level extension of the WBM accurately describes the elastodynamic membrane behaviour, Fig. 18 shows a contour of the structural forced displacement amplitude at 18.4 kHz obtained using both quadratic FE model 10 (6.392.000 DOFs) and a multi-level WBM model containing only 512 basis functions in the displacement expansion (172 bounded and 21 unbounded dilatational DOFs and 284 bounded and 35 unbounded rotational wave functions). This frequency is well within the mid-frequency range, since the membrane has 96 uncoupled modes below it. The results show that the multi-level WBM is capable of accurately describing the spatial distribution of the dynamic displacement field within a perforated membrane.

In order to compare the computational efficiency of the multi-level WBM and the FEM in both the low- and mid-frequency range, a convergence analysis is performed. For all the models described above, the forced structural displacements at 1 kHz, 8.75 kHz and 19.25 kHz are calculated in the four response points indicated in Fig. 17. The symmetric location of these points with respect to the problem geometry allows detection of possible difficulties of the multi-level method to describe symmetric solution fields since the symmetry of the problem definition must inherently result in symmetric responses. The first frequency is in the low-frequency range, the second one is in the region where the low- and mid-frequency range overlap and the third one is far within the mid-frequency range. Based on the calculated displacement values, the average relative prediction error ε_{av} for the forced response amplitude is defined as:

$$\varepsilon_{av}=\frac{1}{4}\sum_{j=1}^{4}\epsilon_j=\frac{1}{4}\sum_{j=1}^{4}\left|\frac{W_{model}(\mathbf{r_j})-W_{ref}(\mathbf{r_j})}{W_{ref}(\mathbf{r_j})}\right|, \tag{68}$$

with $W_{model}(\mathbf{r_j})$ the calculated displacement amplitude and $W_{ref}(\mathbf{r_j})$ the reference displacement amplitude at each of the response locations $\mathbf{r_j}$ and the displacement amplitude defined as $W_{\bullet}=\sqrt{w_{\bullet x}^2+w_{\bullet y}^2}$. These results are plotted against the CPU times needed to solve the different models. Only frequency-dependent

Table 3
FEM model properties for elastodynamic verification example 1.

Model number	h_{max} [m]	Linear FE models		Quadratic FE models	
		#DOFs (=2×#nodes)	t_{solve} [s]	#DOFs (=2×#nodes)	t_{solve} [s]
FE 1	0.02500	14,080	0.3	41,920	1.4
FE 2	0.02000	21,600	0.4	64,400	2.4
FE 3	0.01500	38,592	0.9	115,240	4.8
FE 4	0.01000	86,400	2.2	258,400	13.3
FE 5	0.00800	134,000	3.8	401,000	22.9
FE 6	0.00600	237,808	7.7	712,088	48.8
FE 7	0.00500	342,400	12.1	1,025,600	80.3
FE 8	0.00400	534,000	21.4	1,600,000	151.1
FE 9	0.00300	948,384	46.0	2,842,488	325.4
FE 10	0.00200	2,132,000	143.1	6,392,000	1,068.6
FE 11	0.00150	3,799,232	321.5	11,392,360	2,802.9
FE 12	0.00125	5,459,200	612.4	16,371,200	4,529.1
FE 13	0.00100	8,536,000	1,028.7	25,600,000	/
FE 14	0.00080	13,330,000	2,105.2	/	/

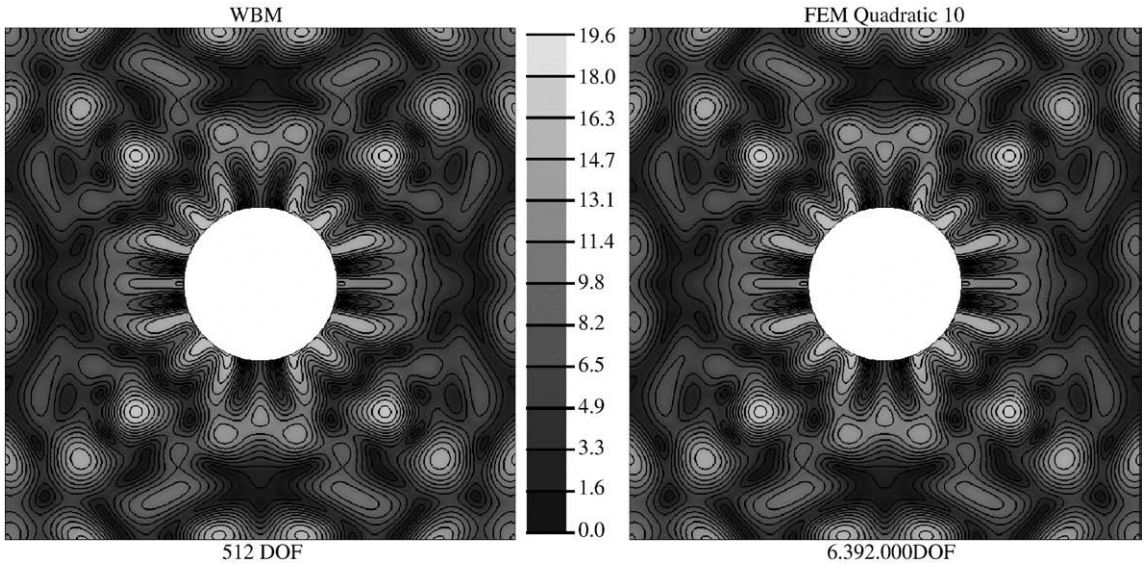

Fig. 18. Elastodynamic verification 1: forced displacement amplitude [10^{-9} m] at 18.4 kHz predicted by the WBM (left) and FEM (right).

operations are taken into account in the calculation time. That means that for the FEM only the time needed to solve the system of equations is given, and for the WBM the time needed to build the WB system matrix as well as the time needed to solve the system of equations are given. The time to build the FE matrices is not taken into account for the FEM, since this effort is frequency independent and negligible when a large number of frequencies is considered.

Fig. 19(a)–(c) compare the convergence rate of the different WB models with that of the FE models in the low- and mid-frequency range. Each subfigure plots the global convergence curve for the quadratic FEM

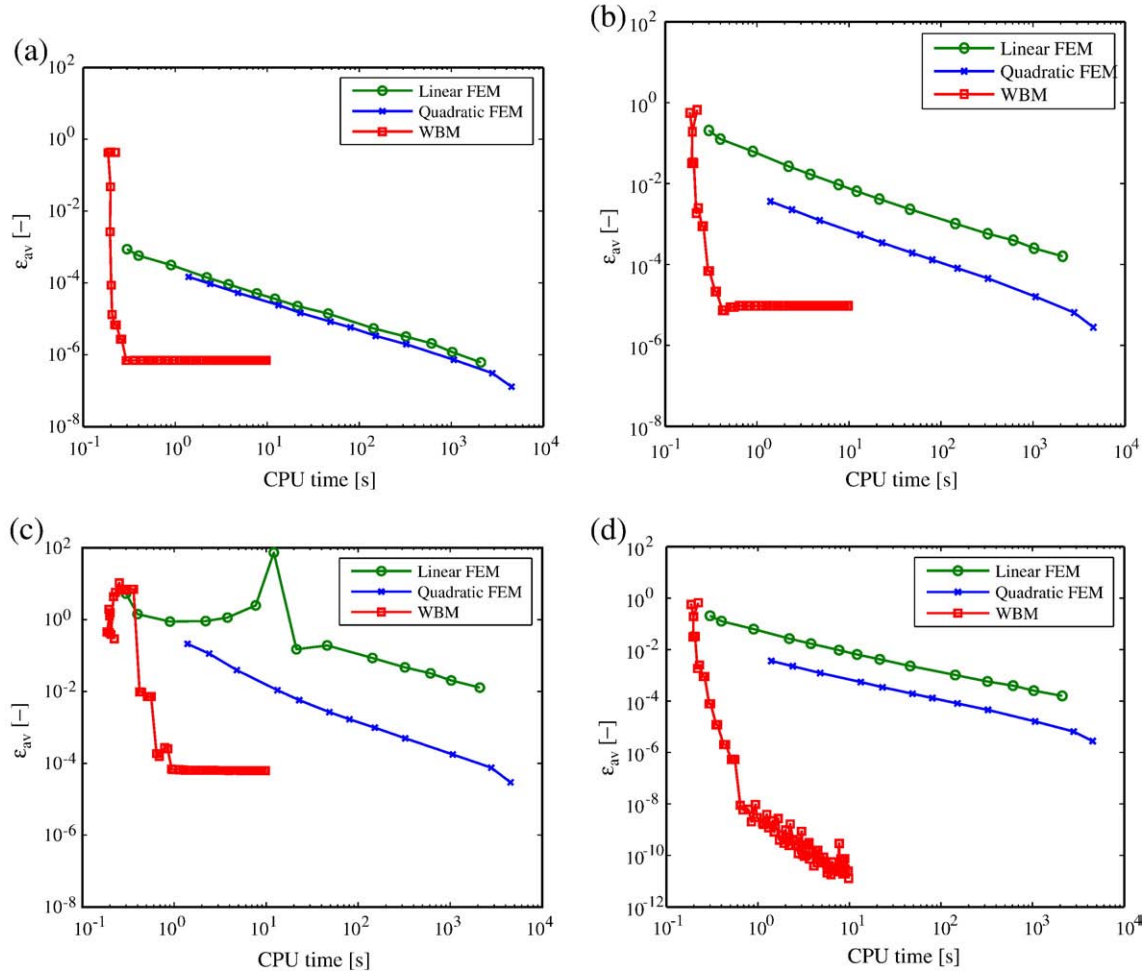

Fig. 19. Elastodynamic verification 1: convergence curves for the linear and quadratic FEM and WBM.

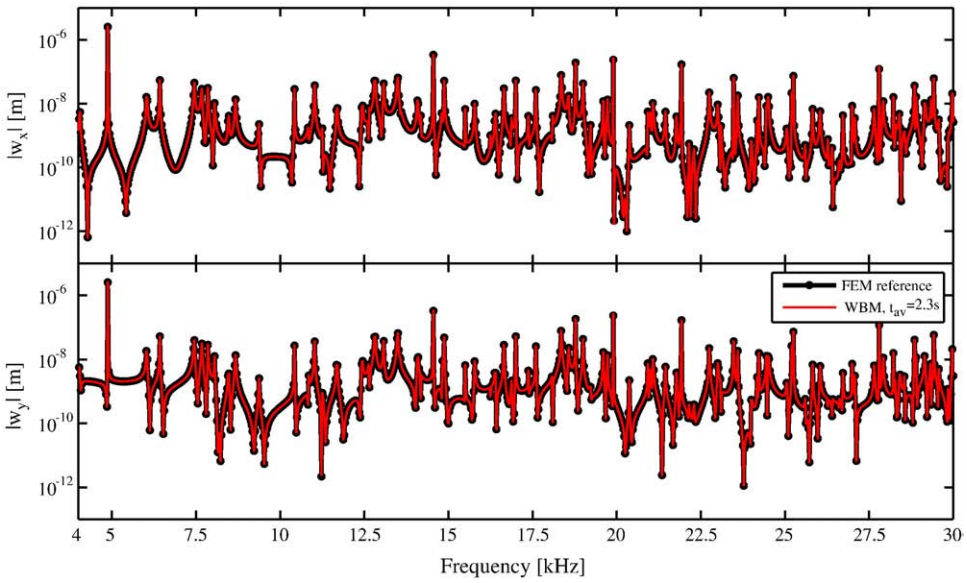

Fig. 20. Elastodynamic verification 1: forced displacement response functions for the response point w_1 predicted by a reference FEM model (thick black line) and the WBM (red line).

(× marker), the linear FEM (○ marker) and the WBM (□ marker). The global curves for the FEM are obtained by incrementally refining the structural elements in the model. The convergence curves for the WB models are calculated by using an increasing number of wave functions (ranging from 30 to 1334 DOFs) to model the structural displacement field. The convergence curves show that, as the number of wave functions increases, the prediction accuracy of the WB models increases until some saturation level is reached after which adding additional wave functions does no longer result in a better prediction accuracy.

For the three frequencies shown here, the WB models converge faster to a certain prediction accuracy as compared to both the linear and quadratic FE models. For the low-frequency case, both the linear and quadratic FE models perform equally well. As the frequency increases, the advantages of using a higher-order FEM scheme become apparent and the quadratic FEM is, for a fixed calculation time, at least 1 to 2 orders of magnitude more accurate. Both the linear and quadratic models show a monotonic convergence behaviour. The WB convergence curves show a very steep decline at very low calculation times, but stabilise at a fixed prediction accuracy of 10^{-4} to 10^{-6} depending on the frequency of interest. This type of convergence behaviour is typically seen when the model which is used as a reference solution has not yet converged to a better accuracy than the model with which it is compared. To show that this is probably the case, Fig. 19(d) shows the convergence curves for the FEM and multi-level WBM methods at 8.75 kHz which are obtained when the finest WBM prediction result is used as reference solution. The FEM convergence curves remain unchanged while the WBM curve no longer saturates but reaches a prediction accuracy of 10^{-11} in approximately 10 cpu s. These results show that the multi-level WB performs clearly better than the linear and quadratic FEM in both the low- and mid-frequency range.

In order to study the behaviour of the different methods in an entire frequency range, the forced structural displacement spectrum between 4 kHz and 30 kHz at response location w_1 is calculated with a multi-level WB model with an average computational load of 1.68 *s* per frequency. This model contains a frequency-dependent number of DOFs which ranges from 219 at 4 kHz to 1104 at 30 kHz ($T=5$). In Fig. 20, the results of these calculations (for both the amplitude of the displacement in the *x*- and *y*-directions) are compared with a reference solution (thick line) obtained with the quadratic FE model 9 in Table 3. The multi-level WBM predictions show a perfect agreement with the reference solution in the entire frequency range. The higher computational efficiency of the WBM is illustrated in Fig. 21, which shows the relative displacement

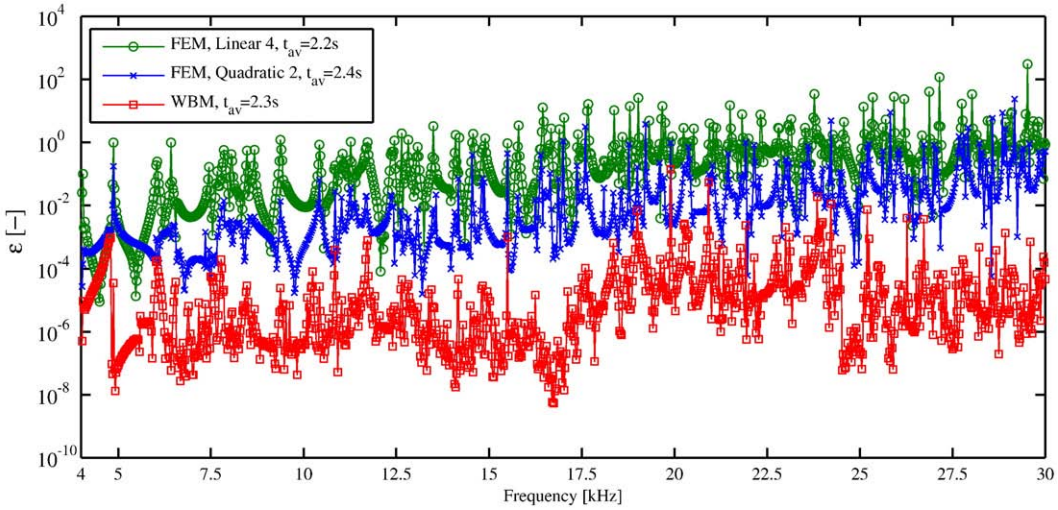

Fig. 21. Elastodynamic verification 1: relative prediction error for the linear and quadratic FEM and WBM as a function of frequency.

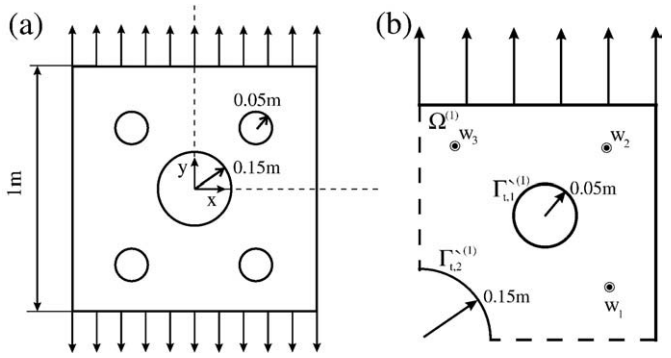

Fig. 22. Elastodynamic verification 2: square plate with 5 circular holes.

amplitude errors in the low- and mid-frequency range for linear FE model 4, quadratic FE model (2) and the multi-level WBM model with respect to a refined WBM reference model. All the models in this comparison have approximately the same computational cost for the full frequency response analysis. The relative prediction errors for the three models are very similar at the lower end of the frequency range, but almost immediately the FEM prediction accuracy begins to deteriorate. The quadratic model suffers less from these effects than the linear model, which is on average one order of magnitude less accurate than the former. The WBM predictions are by far the most accurate and the errors for this model are for all frequencies at least two orders of magnitude smaller than those for the quadratic FEM. This clearly shows the advantageous convergence properties of the proposed method.

5.5. Numerical verification example 2: symmetric membrane containing multiple circular holes

In a second verification example, the multi-level concept is applied to the problem shown in Fig. 22(a). A plate with a thickness of 0.001 m which contains five holes is excited by a unit line load at the top and at the bottom. All other edges are free. The material of the plate is an aluminium alloy with the following parameters: $E=70\cdot10^9$ N/m^2, $\nu=0.3$, $\rho=2{,}790$ kg/m^3.

The symmetry of the problem makes it possible to model only a quarter of the problem. When using symmetry boundary conditions a square plate with a circular hole in the middle and a quarter of a circle removed from one corner remains, see Fig. 22(b). The following response points are considered: $w_1(0.394\,\text{m}, 0.106\,\text{m})$, w_2 (0.394 m, 0.394 m) and w_3(0.106 m, 0.394 m).

With the traditional WBM it would not be possible to model this plate accurately, since it is impossible to divide the problem into convex subdomains. The circular hole and the quarter circle can be approximated by a large number of straight edges, but that would lead to a rough approximation and a large number of subdomains, which jeopardises the computational efficiency of the WBM. With the multi-level approach, it is possible to use only one bounded and two unbounded domains, which are coupled at the boundaries. One unbounded level is used for the circle and one for the quarter circle. The truncation circle of the unbounded level corresponding to the quarter circle lies partly out of the problem domain. Only the part inside the bounded domain is considered in the weighted residual formulation. It will be shown in this example that this is sufficient and that it does not disturb the convergence of the method.

The various WB models are created in a similar fashion as in the previous example. As point of comparison, the perforated membrane is modelled using both linear and quadratic FEM models, the details of which are given in Table 4.The most detailed quadratic FE model (model number (7)) serves as a reference solution when comparing the computational accuracy of the different models at a single frequency.

To illustrate that the multi-level extension of the WBM describes the elastodynamic membrane behaviour accurately, Fig. 23 shows a contour of the structural forced displacement amplitude at 18.4 kHz obtained using bothquadratic FE model 6 (4.035.038 DOFs) and a multi-level WBM model containing only 406 basis functions in the displacement expansion (188 bounded and 40 unbounded dilatational DOFs and 116 bounded and 62 unbounded rotational wave functions). The results show that the multi-level WBM is capable of accurately describing the spatial distribution of the dynamic displacement field within the perforated membrane.

In order to compare the computational efficiency of the multi-level WBM and the FEM in both the low- and mid-frequency range, a second convergence analysis is performed. The forced structural displacements at 1 kHz, 8.75 kHz and 25.75 kHz are calculated in the three response points indicated in Fig. 22(b). Based on the calculated displacement values, the average relative prediction error ε_{av} for the forced response can be computed similar to the previous verification example:

$$\varepsilon_{av} = \frac{1}{3}\sum_{j=1}^{3}\epsilon_j = \frac{1}{3}\sum_{j=1}^{3}\left|\frac{W_{model}(\mathbf{r_j})-W_{ref}(\mathbf{r_j})}{W_{ref}(\mathbf{r_j})}\right|, \tag{69}$$

These results are plotted against the CPU times needed to solve the different models. Again only frequency-dependent operations are taken into account in the calculation time.

Fig. 24(a)–(c) compare the convergence rate of the different WB models with that of the FE models in the low- and mid-frequency range. Each subfigure plots the global convergence curve for the quadratic FEM (× marker), the linear FEM (○ marker) and the WBM (□ marker). The convergence curves for the WB models are calculated by using an increasing number of wave functions (ranging from 36 to 1508 DOFs) to model the structural displacement field.

For the three frequencies shown here, the WB models converge faster to a certain prediction accuracy as compared to both the linear and quadratic FE models. Both the linear and quadratic models show an (almost) monotonic convergence behaviour. The WB convergence curves show a very steep decline, but again stabilise at a fixed prediction accuracy of 10^{-5} to 10^{-6} depending on the frequency of interest. As for the previous numerical example, it is likely that the model which is used as a reference solution has not yet converged to a better accuracy than the model with which it is compared. To show that this is probably the case, Fig. 24(d) shows the convergence curves

Table 4
FEM model properties for elastodynamic verification example 2.

Model number	h_{max} [m]	Linear FE models		Quadratic FE models	
		#DOFs (=2×#nodes)	t_{solve} [s]	#DOFs (=2×#nodes)	t_{solve} [s]
FE 1	0.02500	4,484	0.03	13,282	0.17
FE 2	0.01000	13,560	0.13	40,382	0.67
FE 3	0.00750	24,114	0.24	71,942	1.37
FE 4	0.00500	54,322	0.69	162,366	4.07
FE 5	0.00250	216,086	4.09	647,054	26.00
FE 6	0.00100	1,346,018	49.20	4,035,038	395.00
FE 7	0.00050	5,371,238	389.20	16,107,678	3,572.70

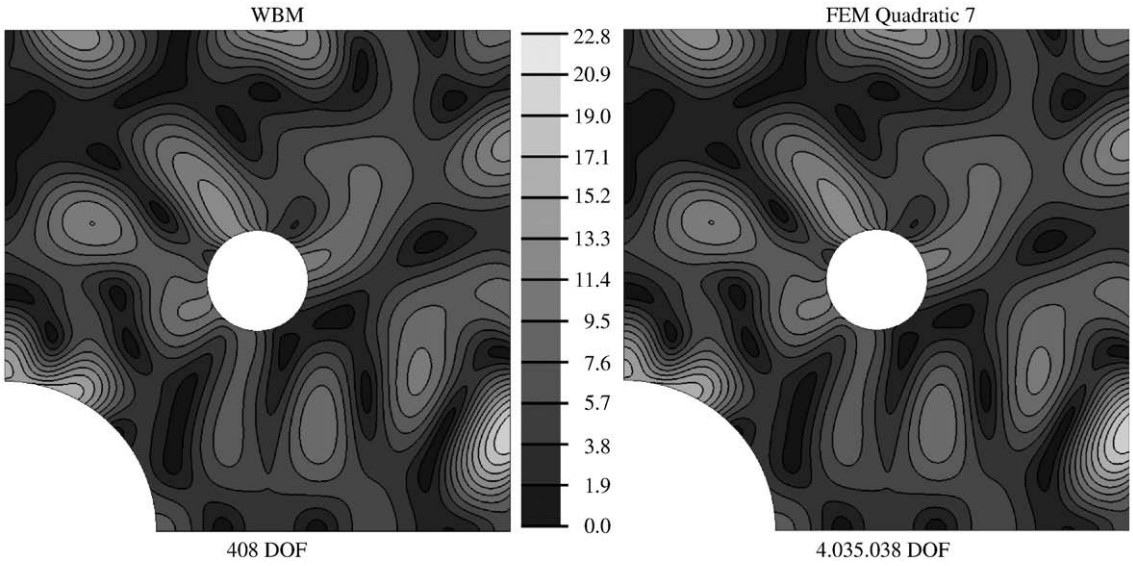

Fig. 23. Elastodynamic verification 2: forced displacement amplitude [10^{-9} m] at 18.4 kHz predicted by the WBM (left) and FEM (right).

for the FEM and multi-level WBM methods at 8.75 kHz which are obtained when the finest WBM prediction result is used as reference solution. The FEM convergence curves remain unchanged while the WBM curve no longer saturates but reaches a prediction accuracy of 10^{-11} in approximately 3 cpu s. These results show that the multi-level WB performs better clearly better than the quadratic and the linear FEM in both the low- and mid-frequency range.

In order to study the behaviour of the different methods in an entire frequency range, the forced structural displacement spectrum between 5 kHz and 30 kHz at response location w_2 is calculated with a multi-level

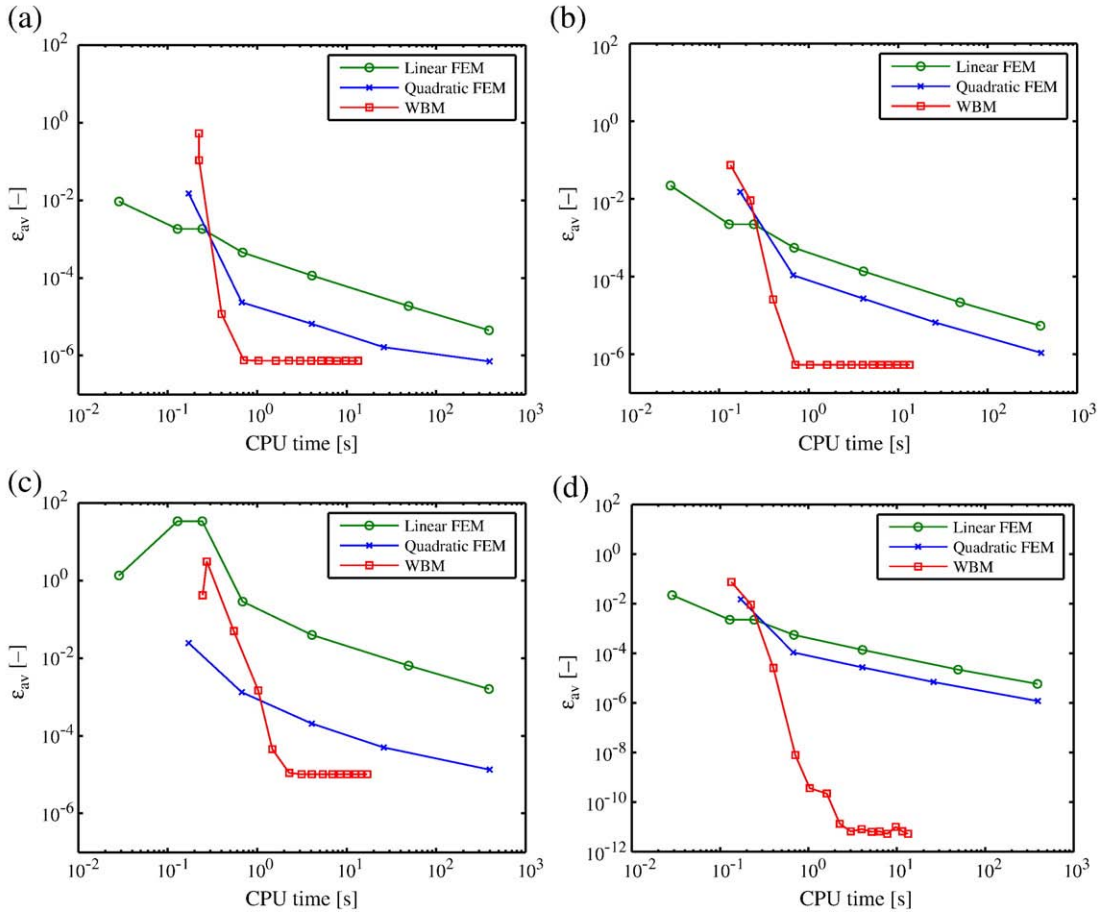

Fig. 24. Elastodynamic verification 2: convergence curves for the linear and quadratic FEM and WBM with FE quadratic model 7 as reference.

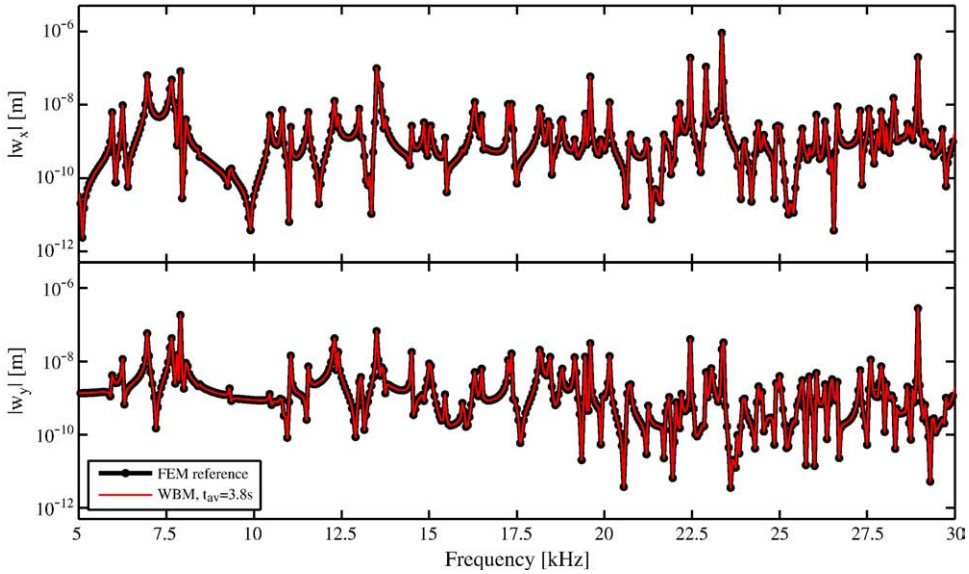

Fig. 25. Elastodynamic verification 2: forced displacement response functions for the response point w_1 predicted by a reference FEM model (thick black line) and the WBM (red line).

WBM model with a calculation time of 3.8 s per frequency, a linear FEM model of 4.1 s per frequency and a quadratic model of 4.1 s per frequency. Fig. 25 compares the WBM results for the displacement amplitude in the *x*- and *y*-directions with a FEM reference solution obtained with quadratic FE model 7 in Table 4. In Fig. 26 the relative displacement amplitude errors, compared to a very accurate WBM calculation, are shown for the three calculations with approximately the same computational load. It can be seen that the linear and quadratic FE calculations show a similar accuracy at low frequencies, but at higher frequencies the accuracy of the linear FEM deteriorates more quickly than the quadratic FEM. Over the entire frequency range, the multi-level WBM calculation is several orders of magnitude more accurate than both linear and quadratic FE models with a comparable computational load.

6. Conclusions

This paper discusses a new multi-level modelling framework, aimed to alleviate or remove some of the geometrical constraints faced when applying the WBM for the study of interior steady-state dynamic problems with multiple inclusions which are governed by a (system of) Helmholtz-type partial differential equations. The main idea of the approach is to consider the multiple objects in a problem as different 'levels' of the problem. Each level considers the reflection and scattering on the boundaries of one particular object, using existing WBM techniques for bounded and unbounded problems. A special compound wave function set and an adapted weighted residual formulation link the different levels together, yielding a single multi-level system, describing the entire problem.

This newly developed modelling framework is first cast in a form which is applicable to a general Helmholtz problem definition. Next, the methodology is presented in more detail for two classes of dynamic problems which are either governed by or can be cast into a Helmholtz-type problem by means of a transformation of the primary field variables. Both for the steady-state interior dynamic behaviour of an acoustic cavity and the elastodynamic deformations of a finite size membrane, suitable wave function expansions and the associated weighted residual formulation for a multi-level WBM model in which all inclusions are circular are presented.

For both problem types the numerical framework is successfully applied to several numerical examples of varying degree of

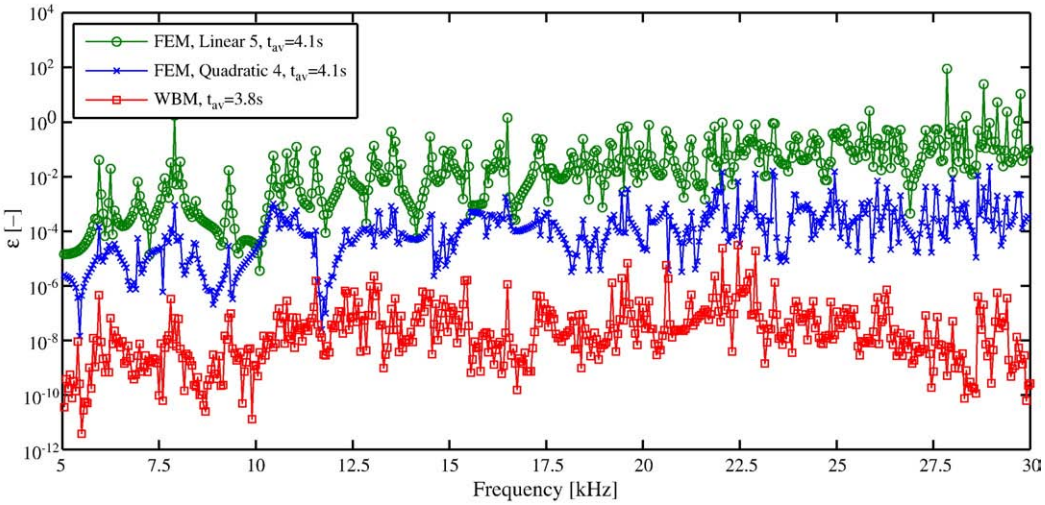

Fig. 26. Elastodynamic verification 2: relative prediction error for the linear and quadratic FEM and WBM as a function of frequency.

complexity, indicating both the excellent accuracy and the superior numerical performance as compared to classical element-based numerical modelling techniques. The reduction in computational load, combined with the lack of pollution errors, makes the WBM particularly suited for the treatment of interior Helmholtz problems with complex inclusion configurations in an extended frequency range.

In the future, this methodology will be applied to more complex Helmholtz problems such as multi-material aggregates in an elastic material and wave propagation problems in unbounded solid media. Also, the general modelling framework will be extended to cope with the influence of perforations on the out of plane bending behaviour of (networks of) flat plates. The application of this methodology to bounded problems containing non-circular inclusions (including the influence of the applied coupling strategies to cope with these types of geometries) and to three dimensional acoustic and elastodynamic problems will be studied.

Acknowledgements

Bert Van Genechten and Karel Vergote are Doctoral Fellows of the Fund for Scientific Research — Flanders (F.W.O.), Belgium.

References

[1] O.C. Zienkiewicz, R.L. Taylor, J.Z. Zhu, P. Nithiarasu, The Finite Element Method — The Three Volume Set, 6th EditionButterworth-Heinemann, 2005.
[2] P. Bouillard, F. Ihlenburg, Error estimation and adaptivity for the finite element method in acoustics: 2d and 3d applications, Computer Methods in Applied Mechanics and Engineering 176 (1–4) (1999) 147–163. doi:10.1016/S0045-7825(98)00334-X.
[3] R. Freymann, Advanced Numerical and Experimental Methods in the Field of Vehicle Structural-Acoustics, Hieronymus Buchreproduktions GmbH, München, 2000.
[4] I. Harari, D. Avraham, High-order finite element methods for acoustic problems, Journal of Computational Acoustics 5 (1997) 33–51. doi:10.1142/S0218396X97000046.
[5] W. Rachowicz, D. Pardo, L. Demkowicz, Fully automatic hp-adaptivity in three dimensions, Computer Methods in Applied Mechanics and Engineering 195 (2006) 4816–4842. doi:10.1016/j.cma.2005.08.022.
[6] S. Challa, High-order accurate spectral elements for wave propagation problems, Clemson University, Mechanical Engineering Department, Master's thesis, 1998.
[7] M.N. Guddati, B. Yue, Modified integration rules for reducing dispersion error in finite element methods, Computer Methods in Applied Mechanics and Engineering 193 (2004) 275–287. doi:10.1016/j.cma.2003.09.010.
[8] L.L. Thompson, P. Kunthong, A residual based variational method for reducing dispersion error in finite element methods, Proceedings of the 2005 ASME International Mechanical Engineering Congress and Exposition, Orlando, Florida, USA, 2005, pp. Paper IMECE2005–80551.
[9] B. Yue, M.N. Guddati, Dispersion-reducing finite elements for transient acoustics, Journal of the Acoustical Society of America 118 (2005) 2132–2141. doi:10.1121/1.2011149.
[10] Y.A. Erlangga, Advances in iterative methods and preconditioners for the Helmholtz equation, Archives of Computational Methods in Engineering 15 (1) (2008) 37–66. doi:10.1007/s11831-007-9013-7.
[11] Y. Saad, Iterative methods for sparse linear systems, 2nd Edition, 2003 SIAM.
[12] R.R. Craig Jr., Structural Dynamics: An Introduction to Computer Methods, John Wiley & Sons, New York Chichester Brisbane Toronto Singapore, 1981.
[13] J.K. Bennighof, M.F. Kaplan, M.B. Muller, M. Kim, Meeting the NVH Computational Challenge: Automated Multi-Level Substructuring, in: Proceedings of the International Modal Analysis Conference XVIII (IMAC18), San Antonio, USA, 2000 pp. 909–915.
[14] A. Kropp, D. Heiserer, Efficient broadband vibro-acoustic analysis of passenger car bodies using an FE-based component mode synthesis approach, Journal of Computational Acoustics 11 (2003) 139–157. doi:10.1142/S0218396X03001870.
[15] D.K. Datta, S. Dey, J.J. Shirron, Scalable Three-Dimensional Acoustics Using hp-finite/infinite elements and FETI-DP, in: Proceedings of the 16th International Domain Decomposition Conference (DDM16), USA, New York, 2005.
[16] C. Farhat, A. Macedo, M. Lesoinne, F.-X. Roux, F. Magoules, A. de La Bourdonnaie, Two-level domain decomposition methods with Lagrange multipliers for the fast iterative solution of acoustic scattering problems, Computer Methods in Applied Mechanics and Engineering 184 (2000) 213–239. doi:10.1016/S0045-7825(99)00229-7.
[17] I. Harari, T.J.R. Hughes, Galerkin/least-squares finite element methods for the reduced wave equation with non-reflecting boundary conditions in unbounded domains, Computer Methods in Applied Mechanics and Engineering 98 (1992) 411–454. doi:10.1016/0045-7825(92)90006-6.
[18] I. Harari, F. Magoules, Numerical investigations of stabilized finite element computations for acoustics, Wave Motion 39 (2004) 339–349. doi:10.1016/j.wavemoti.2003.12.001.
[19] I.M. Babuska, S.A. Sauter, Is the Pollution Effect of the FEM Avoidable for the Helmholtz Equation Considering High Wave Numbers? SIAM Journal on Numerical Analysis 34 (1997) 2392–2423. doi:10.1137/S0036142994269186.
[20] O. Cessenat, B. Desprès, Using plane waves as base functions for solving time harmonic equations with the ultra weak variational formulation, Journal of Computational Acoustics 11 (2) (2003) 227–238. doi:10.1142/S0218396X03001912.
[21] T. Huttunen, P. Monk, J.P. Kaipio, Parallelized UWVF method for 3D Helmholtz problems, Proceedings of the European Congress on Computational Methods in Applied Sciences and Engineering, Jyvaskyla, Finland, 2004, p. CDrom.
[22] C. Farhat, I. Harari, L.P. Franca, The discontinuous enrichment method, Computer Methods in Applied Mechanics and Engineering 190 (2001) 6455–6479. doi:10.1016/S0045-7825(01)00232-8.
[23] I. Harari, N. Makmel, Dispersion analysis of the discontinuous enrichment method for plane-strain elasticity, International Journal for Computational Methods in Engineering Science & Mechanics 10 (2009) 303–316. doi:10.1080/15502280903023157.
[24] C. Farhat, I. Harari, U. Hetmaniuk, The discontinuous enrichment method for multiscale analysis, Computer Methods in Applied Mechanics and Engineering 192 (2003) 3195–3209. doi:10.1016/S0045-7825(03)00344-X.
[25] C. Farhat, I. Harari, U. Hetmaniuk, A discontinuous Galerkin method with Lagrange multipliers for the solution of Helmholtz problems in the mid-frequency range, Computer Methods in Applied Mechanics and Engineering 192 (2003) 1389–1419. doi:10.1016/S0045-7825(02)00646-1.
[26] R. Tezaur, C. Farhat, Three-dimensional discontinuous Galerkin elements with plane waves and Lagrange multipliers for the solution of mid-frequency Helmholtz problems, International Journal for Numerical Methods in Engineering 66 (5) (2006) 796–815. doi:10.1002/nme.1575.
[27] T. Strouboulis, I. Babuska, R. Hidajat, The generalized finite element method for Helmholtz equation: Theory, computation, and open problems, Computer Methods in Applied Mechanics and Engineering 195 (37–40) (2006) 4711–4731. doi:10.1016/j.cma.2005.09.019.
[28] T. Strouboulis, I. Babuska, R. Hidajat, The generalized finite element method for Helmholtz equation, Part II: Effect of choice of handbook functions, error due to absorbing boundary conditions and its assessment, Computer Methods in Applied Mechanics and Engineering 197 (5) (2008) 364–380. doi:10.1016/j.cma.2007.05.019.
[29] T. Strouboulis, K. Copps, I. Babuska, The generalized finite element method, Computer Methods in Applied Mechanics and Engineering 190 (2001) 4081–4193. doi:10.1016/S0045-7825(01)00188-8.
[30] N. Sukumar, D.L. Chopp, N. Moës, T. Belytschko, Modeling holes and inclusions by level sets in the extended finite-element method, Computer Methods in Applied Mechanics and Engineering 190 (46–47) (2001) 6183–6200. doi:10.1016/S0045-7825(01)00215-8.
[31] T. Strouboulis, K. Copps, I. Babuska, The generalized finite element method: an example of its implementation and illustration of its performance, International journal for numerical methods in engineering 47 (2000) 1401–1417. doi:10.1002/(SICI)1097-0207(20000320)47:8%3C1401::AID-NME835%3E3.0.CO;2-8.
[32] R. Piltner, Special finite elements with holes and internal cracks, International journal for numerical methods in engineering 21 (1985) 1471–1485. doi:10.1002/nme.1620210809.
[33] R. Piltner, Recent developments in the trefftz method for finite element and boundary element applications, Advances in Engineering Software 24 (1995) 107–115. doi:10.1016/0965-9978(95)00063-1.
[34] M. Dhanasekar, J. Han, Q. Qin, A hybrid-trefftz element containing an elliptic hole, Finite elements in analysis and design 42 (2006) 1314–1323. doi:10.1016/j.finel.2006.06.008.
[35] T. Hughes, J. Cottrell, Y. Bazilevs, Isogeometric analysis: Cad, finite elements, nurbs, exact geometry and mesh refinement, Computer Methods in Applied Mechanics and Engineering 194 (39–41) (2005) 4135–4195. doi:10.1016/j.cma.2004.10.008.
[36] J. Cottrell, A. Reali, Y. Bazilevs, T. Hughes, Isogeometric analysis of structural vibrations, Computer Methods in Applied Mechanics and Engineering 195 (41–43) (2006) 5257–5296. doi:10.1016/j.cma.2005.09.027.
[37] O. Von Estorff, Boundary Elements in Acoustics: Advances and Applications, WITpress, 2000.
[38] S. Marburg, Six boundary elements per wavelength: is that enough? Journal of Computational Acoustics 10 (2002) 25–51. doi:10.1142/S0218396X02001401.
[39] E. Trefftz, Ein gegenstuck zum ritzschen verfahren, in: Second International Congress on Applied Mechanics, Zürich, Switserland, 1926 pp. 131–137.
[40] B. Pluymers, B. Van Hal, D. Vandepitte, W. Desmet, Trefftz-based methods for time-harmonic acoustics, Archives of Computational Methods in Engineering 14 (4) (2006) 343–381. doi:10.1007/s11831-007-9010-x.
[41] W. Desmet, A wave based prediction technique for coupled vibro-acoustic analysis, K.U. Leuven, division PMA, PhD. thesis 98D12.http://www.mech.kuleuven.be/mod/wbm/phd.
[42] W. Desmet, B. Van Hal, P. Sas, D. Vandepitte, A computationally efficient prediction technique for the steady-state dynamic analysis of coupled vibro-acoustic systems, Advances in Engineering Software 33 (2002) 527–540. doi:10.1016/S0965-9978(02)00062-5.
[43] B. Pluymers, W. Desmet, D. Vandepitte, P. Sas, Application of an efficient wave based prediction technique for the analysis of vibro-acoustic radiation problems, Journal of Computational and Applied Mathematics 168 (2004) 353–364. doi:10.1016/j.cam.2003.05.020.
[44] B. Pluymers, W. Desmet, D. Vandepitte, P. Sas, On the use of a wave based prediction technique for steady-state structural-acoustic radiation analysis, Computer Modeling in Engineering & Sciences 7 (2) (2005) 173–184.

[45] B. Pluymers, B. Van Hal, D. Vandepitte, W. Desmet, Trefftz-based methods for time-harmonic acoustics, Archives of Computational Methods in Engineering 14 (4) (2007) 343–381. doi:10.1007/s11831-007-9010-x.
[46] C. Vanmaele, D. Vandepitte, W. Desmet, An efficient wave based prediction technique for plate bending vibrations, Computer Methods in Applied Mechanics and Engineering 196 (33–34) (2007) 3178–3189. doi:10.1016/j.cma.2007.03.002.
[47] C. Vanmaele, D. Vandepitte, W. Desmet, An efficient wave based prediction technique for dynamic plate bending problems with corner stress singularities, Computer Methods in Applied Mechanics and Engineering 198 (30–32) (2009) 2227–2245. doi:10.1016/j.cma.2009.01.015.
[48] B. Van Genechten, B. Bergen, B. Pluymers, D. Vandepitte, W. Desmet, A novel modelling approach for sound propagation analysis in a multiple scatterer environment, The Journal of the Acoustical Society of America 123 (5) (2008) 10.1121/1.2935336.
[49] B. Van Genechten, D. Vandepitte, W. Desmet, A trefftz-based numerical modelling framework for helmholtz problems with complex multiple scatterer configurations, submitted to Journal of Computational Physics.
[50] J.T. Chen, Y.T. Lee, S.C. Shieh, Revisit of two classical elasticity problems by using the trefftz method, Engineering Analysis with Boundary Elements 33 (2009) 890–895. doi:10.1016/j.enganabound.2008.12.003.
[51] P. Ladevèze, L. Blanc, P. Rouch, C. Blanzé, A multiscale computational method for medium-frequency vibrations of assemblies of heterogeneous plates, Computers & Structures 81 (12) (2003) 1267–1276. doi:10.1016/S0045-7949(03)00041-5.
[52] L. Blanc, C. Blanzé, P. Rouch, A multiscale trefftz computational method for medium-frequency vibrations of assemblies of heterogeneous plates with uncertainties, Computers & Structures 85 (10) (2007) 595–605. doi:10.1016/j.compstruc.2006.08.078.
[53] H. Riou, P. Ladevèze, P. Rouch, Extension of the variational theory of complex rays to shells for medium-frequency vibrations, Journal of Sound and Vibration 272 (2004) 341–360. doi:10.1016/S0022-460X(03)00775-2.
[54] M. Stojek, Finite *T*-elements for the Poisson and Helmholtz equations, Ecole polytechnique federal de Lausanne, PhD. thesis, 1996.
[55] M. Stojek, Least-squares Trefftz-type elements for the Helmholtz equation, International Journal for Numerical Methods in Engineering 41 (1998) 831–849. doi:10.1002/(SICI)1097-0207(19980315)41:5<831::AID-NME311>3.0.CO;2-V.
[56] D. Colton, R. Kress, Inverse acoustic and electromagnetic scattering theory, 2nd EditionSpringer-Verlag, Berlin, Heidelbert, New York, 1998.
[57] P. Monk, D.-Q. Wang, A least-squares method for the helmholtz equation, Computer Methods in Applied Mechanics and Engineering 175 (1–2) (1999) 121–136. doi:10.1016/S0045-7825(98)00326-0.
[58] C. Farhat, I. Harari, U. Hetmaniuk, A discontinuous galerkin method with lagrange multipliers for the solution of helmholtz problems in the mid-frequency regime, Computer Methods in Applied Mechanics and Engineering 192 (11–12) (2003) 1389–1419. doi:10.1016/S0045-7825(02)00646-1.
[59] I. Herrera, Boundary Methods: An Algebraic Theory, Pitman Adv. Publ. Program, London, 1984.
[60] B. Van Hal, Automation and performance optimization of the wave based method for interior structural-acoustic problems, K.U.Leuven, division PMA, PhD. thesis 2004D07, 2004.http://www.mech.kuleuven.be/mod/wbm/phdhttp://www.mech.kuleuven.be/mod/wbm/phd.
[61] T. Huttunen, P. Gamallo, R.J. Astley, Comparison of two wave element methods for the Helmholtz problem, Communications in Numerical Methods in Engineering 25 (2009) 35–52. doi:10.1002/cnm.1102.
[62] A.P. Zielinski, I. Herrera, Trefftz method: fitting boundary conditions, International Journal for Numerical Methods in Engineering 24 (1987) 871–891. doi:10.1002/nme.1620240504.
[63] C.F. Gerald, P.O. Wheatley, Applied Numerical Analysis, seventh editionAddison-Wesley Publishing Company, 2003.
[64] B. Van Hal, W. Desmet, D. Vandepitte, P. Sas, Application of the efficient wave based prediction technique for the steady-state dynamic analysis of flat plates, Proceedings ISMA25 - Noise and Vibration Engineering, Leuven, Belgium, 2000, pp. 607–614, http://www.isma-isaac.be/publications/PMA.
[65] C. Vanmaele, Development of a wave based prediction technique for the efficient analysis of low- and mid-frequency structural vibrations, K.U.Leuven, division PMA, PhD. thesis 2007D11, 2007.http://www.mech.kuleuven.be/mod/wbm/phd.
[66] J.M. Varah, A practical examination of some numerical methods for linear discrete ill-posed problems, SIAM Review 21 (1979) 100–111. doi:10.1137/1021007.
[67] J.M. Varah, Pitfalls in the numerical solution of linear ill-posed problems, SIAM Journal on Scientific and Statistical Computing 4 (1983) 164–176.
[68] J. Dominguez, Boundary Elements in Dynamics, Computational Mechanics Publications, 1993.
[69] B. Pluymers, Wave based modelling methods for steady-state vibro-acoustics, K.U. Leuven, division PMA, PhD. thesis 2006D04.http://www.mech.kuleuven.be/mod/wbm/phd.
[70] J.-D. Benamou, B. Desprès, A domain decomposition method for the helmholtz equation and related optimal control problems, Journal of Computational Physics 136 (1) (1997) 68–82. doi:10.1006/jcph.1997.5742.
[71] V.D. Kupradze, T.G. Gegelia, M.O. Basheleishvili, Three-dimensional problems of the mathematical theory of elasticity and thermoelasticity, Vol. 25 of North-Holland series in applied mathematics and mechanics, North-Holland, 1979.
[72] P.A. Martin, Multiple Scattering, Interaction of Time-Harmonic Waves with N obstacles, Vol. 107 of Encyclopedia of Mathematics and its Applications, Cambridge University Press, 2006.